

# Magnetic Jets from Swirling Disks

D. Lynden-Bell<sup>1,2</sup>

<sup>1</sup>*Institute of Astronomy, The Observatories, Cambridge, CB3 0HA*

<sup>2</sup>*Clare College*

This version dated 24 January 2006, revised 3 February 2006, revised following reviewer’s comments 20 March 2006

## ABSTRACT

A broad swathe of astrophysical phenomena, ranging from tubular planetary nebulae through Herbig-Haro objects, radio-galaxy and quasar emissions to gamma-ray bursts and perhaps high-energy cosmic rays, may be driven by magnetically-dominated jets emanating from accretion disks. We give a self-contained account of the analytic theory of non-relativistic magnetically dominated jets wound up by a swirling disk and making a magnetic cavity in a background medium of any prescribed pressure,  $p(z)$ . We solve the time-dependent problem for any specified distribution of magnetic flux  $P(R, 0)$  emerging from the disk at  $z = 0$ , with any specified disk angular velocity  $\Omega_d(R)$ . The physics required to do this involves only the freezing of the lines of force to the conducting medium and the principle of minimum energy.

In a constant pressure environment the magnetically dominated cavity is highly collimated and advances along the axis at a constant speed closely related to the maximum circular velocity of the accretion disk. Even within the cavity the field is strongly concentrated toward the axis. The twist in the jet’s field  $\langle B_\phi \rangle / \langle |B_z| \rangle$  is close to  $\sqrt{2}$  and the width of the jet decreases upwards. By contrast when the background pressure falls off with height with powers approaching  $z^{-4}$  the head of the jet accelerates strongly and the twist of the jet is much smaller. The width increases to give an almost conical magnetic cavity with apex at the source. Such a regime may be responsible for some of the longest strongly collimated jets. When the background pressure falls off faster than  $z^{-4}$  there are no quasi-static configurations of well twisted fields and the pressure confinement is replaced by a dynamic effective pressure or a relativistic expansion. In the regimes with rapid acceleration the outgoing and incoming fields linking the twist back to the source are almost anti-parallel so there is a possibility that magnetic reconnections may break up the jet into a series of magnetic ‘smoke-rings’ travelling out along the axis.

**Key words:** jets, MHD, Cosmic Rays

## 1 INTRODUCTION

### 1.1 Orders of magnitude – the voltages generated

We consider accretion disks of bodies in formation when the differential rotation drags around magnetic field lines. Although the moving magnetic fields inevitably generate electric fields, the resulting EMFs are perpendicular to the magnetic fields in the perfect conduction approximation. Such EMFs do not accelerate particles to high energies. However the world is not a perfect place; in regions where perfect MHD predicts very high current densities there may be too few charge carriers to carry those currents. In those regions perfect conductivity is not a good approximation and the fields are modified to allow an electric field component along the magnetic field so that the larger current can be generated by the few charge carriers available. With this background idea it becomes interesting to get rough estimates of EMFs that are likely to be around whatever their direction. It turns out that these EMFs scale with  $(v/c)^3$  where  $v$  is the maximum velocity in the accretion disk and is independent of the size or mass of the system. Relativistic systems in formation, however small, can generate EMFs whose voltages at least match those of the highest energy cosmic rays. However the timescales over which these systems persist and the total energies available over those time scales do of course depend on the mass of the system. Very crude estimates of

the EMFs can be made as follows. Let us suppose that there is a central object, a star or a black hole, of mass  $M$  surrounded by an accretion disk of mass  $\zeta M$ . Further let us suppose that a small fraction  $\eta$  of the binding energy of the accretion disk is converted into magnetic field energy. Letting  $R$  be the inner radius of the disk we put  $(4\pi/3)R^3(B^2/(8\pi)) = G\zeta\eta M^2/R$  so  $B = (6\zeta\eta/G)^{1/2}v^2/R$ , where  $v^2 = GM/R$ . Fields of a few hundred Gauss are found in T Tauri stars, so putting  $R = 10^{11}\text{cm}$   $v = 300\text{km/s}$  we find  $\zeta\eta = 10^{-11}$ . We shall use this dimensionless number to make estimates elsewhere. Now the EMF generated around a circuit that goes up the axis and back to the disk around a field line and finally along the disk back to the centre is about  $(v/c)BR$  in esu and 300 times that in volts so  $\text{EMF} = 300 (6\zeta\eta/G)^{1/2}(v/c)^3c^2 = (v/c)^3 10^{22}$  volts. Kronberg et al (2004) considered such accelerative processes in radio galaxies.

Again only a fraction of this voltage will be available to accelerate particles; in the exact flux freezing case it is ALL perpendicular to the fields, nevertheless it is an estimate of what might be available where the perfect conductivity approximation breaks down. Although the argument is crude the answer is interesting in that it suggests that cosmic rays generated in microquasars may reach the same individual particle energies as those generated in quasars and radio galaxies which may match the highest cosmic ray energies.

## 1.2 Jets

Curtis photographed the jet in M 87 from the Lick Observatory in 1918. While it was soon found to be blue, the emission process was not understood despite Schott's detailed calculations of synchrotron radiation in his 1912 book. Finally after Shklovskii introduced this emission mechanism into astrophysics Baade (1956) showed the jet to be highly polarized which clinched it. Although Ryle's Cambridge group (1968) found many double radio lobes around large galaxies the next obvious jet came with the identification of the first quasar 3C273 in which the dominant radio source is not at the nucleus but at the other end of the optical jet (Hazard, Mackey & Shimmins 1963; Schmidt 1963). There were difficulties in understanding the powering of the radio lobes of galaxies. If all the energy were present as the lobes expanded outwards there would be more bright small ones. Finally this led Rees (1971) to suggest that the lobes must be continuously powered by as-yet-unseen jets feeding energy into the visible lobes. As radio astronomy moved to higher frequencies with greater resolution these jets duly appeared in both radio galaxies and quasars. All the above jets have dynamically significant magnetic fields seen via their synchrotron radiation; a particularly fine study of one, Hercules A, is found in Gizani & Leahy (2003). Magnetic fields are less obvious in the Herbig-Haro objects first found in star-forming regions in 1951. However it took the development of good infra-red detectors before the heavy obscuration was penetrated in the 1980s to reveal the jets feeding the emission. These jets have velocities of one or two hundred km/s, far less than the  $0.1c - c$  speeds of the extragalactic jets. The jets around young stars are seen to be perpendicular to the accretion discs that generate them. Since the giant black-hole accretion disk theory of quasars Salpeter (1964), Lynden-Bell (1969), Bardeen (1970), Lynden-Bell & Rees (1971) Shakura & Sunyaev (1973, 1976) many have come to believe that the radio galaxies and quasars likewise have jets perpendicular to their inner disks. However it was not until the wonderful work on megamasers (Miyoshi et al. 1995) that such inner disks around black holes were definitively confirmed. In 1969 when I predicted that they would inhabit the nuclei of most major galaxies including our own, M31, M32, M81, M87, etc., the idea was considered outlandish, but now most astronomers take it for granted. Fine work by Kormendy (1995) and others on external galaxies and the beautiful results of Genzel (2003) and Ghez (2004) on our own has totally transformed the situation. Meanwhile many jets have been found in objects associated with dying stars, SS433 and the micro-quasars Mirabel & Rodriguez (1999) being prominent examples within the Galaxy. Less energetic but more beautiful examples may be the tubular planetary nebulae that are associated with accretion discs of central mass-exchanging binary stars. These were brought to my attention by Mark Morris and recent evidence indicates that magnetism is important here too (Vlemmings et al 2006). Much more spectacularly the  $\gamma$ -ray bursts are now thought to come from accretion-disks around black holes within some supernova explosions. Poynting flows of electromagnetic energy appear to be one of the best ways of extracting the energy from beneath the baryons that would otherwise absorb the  $\gamma$ -rays, Uzdensky & MacFadyen (2006). Jets and collimated outflows have also been invoked for giant stars. Remarkable examples are R Aquarii (Michalitsanos et al. 1988) and the Egg nebula (Cohen et al. 2004) and the collimated outflow in IRG 10011 (Vinković 2004).

The systematic features of these diverse objects are that an accretion disk is present and the jet emerges along the rotation axis of the inner disk. Magnetic fields are important in the radio objects and may be important in all. The jet velocities are strongly correlated with the escape velocities and therefore with the circular velocities in the disk close to the central object. In very collapsed objects these velocities are relativistic but in star-forming regions the jet velocities are less than  $10^{-3}c$ . The obvious similarity of the jet structures and collimation despite such velocity differences strongly suggest that relativity is not a determining factor in the making of these jets. The thesis that I put forward in 1996 (paper II) and repeat here, is that all these jets are magnetically driven, the common feature being that the Poynting flux dominates the energy transport in the jet. However I do not exclude the possibility of material being entrained as the jet makes its way through the material that surrounds it. Nevertheless we consider that magnetism is the driver and the prime reason for collimation is the magnetic twisting combined with a weak external pressure which is dynamically enhanced by inertia. It is the electromagnetic field that generates the relativistic particles in radio jets so, even if their total energies evolve to become comparable, the magnetic

energy comes first and drives the whole phenomenon. While this paper is concerned with jets from systems with accretion disks, the jets near pulsars are probably closely related. There the magnetic field is rotated by the neutron star but the weaker field at large radii may be heavily loaded by the inertia close to the light cylinder. Field lines may be twisted from below far faster than they can rotate across the light cylinder. The resulting twisting up of the field within the cylinder may result in jet phenomena with similarities to those described here.

The problem of jet collimation was emphasised by Wheeler (1971) at the Vatican Conference on the Nuclei of Galaxies in 1970. He drew attention to the computations of Leblanc & Wilson (1970) who found a remarkable jet generated on the axis of a rotating star in collapse. This may be hailed as the first gamma-ray burst calculation and the magnetic cavities discussed here are in essence analytic calculations based on the same mechanism. We have concentrated on the simplest case of force-free magnetic fields within the cavity. In earlier work others produced good collimation by twisting up a magnetic field that was imposed from infinity. An early paper on this was by Lovelace (1976) and the rather successful simulations of Shibata & Uchida (1985, 1986) are based on this theme. I consider that the imposition of a straight field from infinity ducks the question of why collimation exists. The straight field imposes it. Much work has concentrated on the hard problem of winds carrying a significant mass flux from a rotating star. This subject is well covered in Mestel's book (1999) Li et al (2001), Lovelace et al (2002) and Sakurai (1987) found a weak asymptotic collimation and Heyvaerts & Norman (2002) have recently concluded a thorough study of the asymptotics of wind collimation. Bogovalov & Tsinganos (2003) have tackled the difficulties of collimating mass loaded flows from central objects and give models with the near-axis part of the flow well collimated despite the centrifugal force. Blandford & Payne (1982) discuss winds launched by centrifugal force. Lovelace & Romanova (2003) Li et al (2006) made numerical calculations based upon the differential winding we proposed in Papers I & II. The stability problems of twisted jets have been tackled in both the linear and non-linear regimes by Appl, Lery & Baty (2000) and Lery, Baty & Appl (2000) while Thompson, Lyutikov and Kulkarni (2002) have applied to magnetars the self-similar fields found in Paper I. In section 5 we find that some magnetic cavities float upwards like bubbles thus fulfilling the ideas of Gull & Northover (1976). The laboratory experiments of Lebedev et al. (2005) give some support for the type of models given here. A fine review of extragalactic jets was given by Begelman et al. (1984). See also the more recent work of Pudritz et al 2006, Ouyed et al 2003.

### 1.3 Outline of this paper

This is the fourth paper of this series and puts a new emphasis on regions in which the ambient pressure decreases with height like  $z^{-4}$ . It also gives detailed analytical solutions of the *dynamical* problem for the first time. Papers II and III concentrated on why there are collimated jets at all. Here we concentrate on the dynamic magnetic configurations generated.

Paper I (Lynden-Bell & Boily 1994) showed that when an inner disk was rotated by 208 degrees relative to an outer disk field lines that had connected them splayed out to infinity in the absence of any confining external pressure. At greater angles there was no torque as the inner and outer disks were magnetically disconnected.

Paper II (Lynden-Bell 1996) demonstrated that inclusion of a weak uniform external pressure led to a strong collimation after many turns with the magnetic field creating towers with jet-like cores whose height grew with each turn. Again the inner disk was rotated rigidly relative to the outer disk.

Paper III (Lynden-Bell 2003) was a refined version of a conference paper (Lynden-Bell 2001). In these the differential rotation of the accretion disk and external pressure variation with height were included and the shape of the magnetic cavity was calculated as a function of time. However the fields were not calculated in detail and the treatment used a static external pressure which was assumed to fall less rapidly than  $z^{-4}$ .

In this Paper IV we show that these quasi-static models are actually dynamically correct provided that the motions generated in the field lines by the twisting of the accretion disk never become relativistic, but we then explore the consequences of the magnetic cavity expanding into a region where the pressure variation approaches  $z^{-4}$ . This results in a dramatic acceleration of the top of the magnetic cavity along a cone whose angle gradually narrows at greater distances. The sudden expansion out to infinity when the twist exceeded a critical angle, found in paper I when there was no confining medium, is still present in modified form when beyond some height the external ambient pressure falls as  $z^{-4}$  or faster; once the field has penetrated to that region there is no longer a quasi-static configuration for the system to go to, so the jet accelerates to reach either dynamic ram-pressure balance whenever the background density falls less fast than  $z^{-6}$  or failing that relativistic speeds.

### 1.4 Dynamics from statics

In the standard MHD approximation the displacement current is neglected so  $\text{curl}\mathbf{B} = 4\pi\mathbf{j}$ . If the magnetic field dominates over any other pressure or inertial forces, then, neglecting those, the magnetic force density has nothing to oppose it, so  $\mathbf{j} \times \mathbf{B} = \mathbf{0}$  and we deduce that the currents flow along the lines of force. This implies that  $\mathbf{j} = \tilde{\alpha}\mathbf{B}$  and as both  $\text{div}\mathbf{B}$  and  $\text{div}\mathbf{j}$  are zero  $\tilde{\alpha}$  is constant along the lines of force.

We shall be considering problems with the normal component of magnetic field specified on an accretion disk at  $z = 0$  and the field does not penetrate the other boundary where an external pressure  $p(z)$  balances  $B^2/8\pi$ . The past motion of the accretion disk has produced a twist in the field-lines which emerge from the disk and return thereto further out. Those with past experience will know that the above conditions supplemented by expressions for  $B_n$  on the disk, the twists  $\Phi$  on each line and  $p(z)$ , serve to define the problem, so the magnetic field is then determined. The other Maxwell equations  $\text{curl} \mathbf{E} = -\partial \mathbf{B}/\partial t$ , and that giving  $\text{div} \mathbf{E}$ , are not needed in the determination of the magnetic field. Notice that all the equations used to find the magnetic field do not involve the time. Thus if we specify the twist angles together with the normal field component on the disk and the boundary pressure  $p(z)$  at any time, the whole field configuration at that time is determined. Now let us suppose that we know how to solve this static problem but that  $B_n(R)$ ,  $\Phi(R)$  and  $p(z)$  are continuously specified as functions of time. Then the solution for the magnetic field in this dynamic problem is found by merely taking the sequence of static problems parameterised by  $t$ . Such a procedure will give us  $\mathbf{B}(\mathbf{r}, t)$  but in the dynamic problem the motions of the lines of magnetic force generate electric fields that must be found also. However these can be found almost as an afterthought because we can determine how the lines of force move and their motion is the  $c\mathbf{E} \times \mathbf{B}/B^2$  drift. Assuming perfect conductivity there is no component of  $\mathbf{E}$  along  $\mathbf{B}$  so  $\mathbf{E} = \mathbf{B} \times \mathbf{u}/c$ . Our knowledge of  $\mathbf{u}$  on the accretion disk tells us how the lines move everywhere, which in turn tells us the electric field.

We conclude that the crux of the problem lies not in difficult and dangerous dynamics but in the staid simplicity and safety of statics. That said we need whole sequences of static solutions that allow us to turn up the twists and parameterise the external pressures. Even the static problem is no walkover and we would have found it impossible to get general solutions were it not for the energy principle that the magnetic field adopts the configuration of minimum energy subject to the flux, twist and pressure constraints imposed at the boundary.

Here we have already demonstrated why an evolution of the magnetic field structure through quasi-static models gives the solution to the dynamic problem. Section 2 details the specification of the relevant static problem and the methods of solving it. In Section 3 we solve it developing further the approximate method of paper III. This gives us the mean fields within magnetic cavities whose shapes we calculate for any prescribed external pressure distribution. Emphasis is placed on solutions that access regions with  $p$  falling like  $z^{-4}$  and the very fast expansions then generated. We then generalise our results to allow for a dynamic ram-pressure and discover the shapes of inertially confined jets. In Section 4 we calculate the detailed magnetic fields within the cavity. Section 5 finds the electric fields generated as the magnetic cavity grows and categorises the types of solution. Section 6 gives exact solutions of special cases with the dynamical electric field also calculated.

## 2 THE MAGNETIC PROBLEMS TO BE SOLVED

A magnetic flux  $P(R_i, 0)$  rises out of an accretion disk on  $z = 0$  at radii up to  $R_i$ . The lines of magnetic force on a tube encircling the flux  $P$  eventually return to the disk at an outer radius  $R_o(P)$  after a total twist around the axis of  $\Phi(P)$ . The magnetic field above the disc is force free with current flowing along the field lines and there is negligible gas pressure within the magnetic-field-dominated cavity. However the magnetic cavity is bounded by a surface at which an external pressure  $p(z)$  is specified. Later we shall consider the case of a dynamical pressure  $p(z, t)$ . Our problem is to find the magnetic field and the shape of the cavity containing it when the functions  $P(R, 0)$ ,  $\Phi(P)$  and  $p(z)$  are specified. Axial symmetry is assumed. We think of  $\Phi$  as due to the disk's past differential rotation and sometimes write  $\Phi(P) = [\Omega_d(R_i) - \Omega_d(R_o)]t = \Omega(P)t$  where the suffix  $d$  refers to the rotation of the disk itself. The equation  $\text{div} \mathbf{B} = 0$  implies that the magnetic field components in cylindrical polar coordinates  $(R, \phi, z)$  may be written in terms of the flux function  $P(R, z)$  which gives the flux through a ring of radius  $R$  at height  $z$ , and the gradient of the azimuthal coordinate  $\phi$ , in the form,

$$\mathbf{B} = (2\pi)^{-1} \nabla P \times \nabla \phi + B_\phi \hat{\phi}. \quad (1)$$

The force-free condition  $4\pi \mathbf{j} \times \mathbf{B} = \text{curl} \mathbf{B} \times \mathbf{B} = 0$  then tells us that  $B_\phi$  takes the form,

$$B_\phi = (2\pi R)^{-1} \beta(P). \quad (2)$$

The function  $\beta$  is constant along each field line (so it is a function of  $P$ ) and must be determined from the solution so that the total twist on that field line is  $\Phi(P)$ . Finally the azimuthal component of the force free condition yields the equation

$$\nabla^2 P - \nabla \ln R^2 \cdot \nabla P = R \frac{\partial}{\partial R} \left( \frac{1}{R} \frac{\partial P}{\partial R} \right) + \frac{\partial^2 P}{\partial z^2} = -\beta'(P) \beta(P) = -8\pi^2 R j_\phi. \quad (3)$$

This is to be solved within an unknown surface  $S$  given by  $R = R_m(z)$  in which the field lies and on which  $\mathbf{B}^2 = 8\pi p(z)$ .

The difficulties of this problem are:

- the equation is non-linear
- the function  $\beta$  in it is not known and can only be determined from  $\Phi(P)$  via the solution.
- the bounding surface  $S$  is unknown.

Luckily there is a different way of tackling these magnetostatic problems. The energy of the magnetic field and of the external gas-pressure must be a minimum subject to the flux and twist conditions on the accretion disk. The pressure energy stored in making a cavity whose area at height  $z$  is  $A(z)$  against an external pressure  $p(z)$  is

$$W_p = \int p(z)A(z)dz. \quad (4)$$

The energy principle that applies even outside axial symmetry is that  $W$  must be a minimum, where

$$8\pi W = \int \left[ \int \int (B_R^2 + B_\phi^2 + B_z^2) R d\phi dR + 8\pi p A \right] dz, \quad (5)$$

and  $\mathbf{B}$  satisfies the flux and twist conditions on  $z = 0$ . Two exact theorems follow; they were proved in paper III by expanding a horizontal slice through the configuration first vertically and then horizontally. Earlier more specialised versions appeared in papers I and II. These theorems are true even without axial symmetry. Defining averages  $\langle \dots \rangle$  over a horizontal plane at height  $z$ ,

$$\langle B_R^2 \rangle + \langle B_\phi^2 \rangle = \langle B_z^2 \rangle + 8\pi \left( p(z) + [A(z)]^{-1} \int_z A(z') [dp/dz'] dz' \right); \quad (6)$$

the final integral from  $z$  up is negative whenever pressure falls at height. Minimum energy for horizontal displacements of the slice gives,

$$\langle B_z^2 \rangle = 8\pi p(z) - (4\pi/A) dW_0(z)/dz, \quad (7)$$

where

$$4\pi W_0 = \int \int B_R B_z R^2 d\phi dR, \quad (8)$$

and the integration is over the plane at height  $z$ .

We shall show presently that after much twisting the magnetic configuration becomes very tall as compared to its width. As no extra radial flux is created the radial field lines become widely spread out over the height of the resultant tower and the gradients with height likewise become small. When we neglect terms involving  $B_R$  equation (7) becomes

$$\langle B_z^2 \rangle = 8\pi p(z), \quad (9)$$

and with a similar neglect in the use of equation (6) we find

$$\langle B_\phi^2 \rangle / (2 - s) = \langle B_z^2 \rangle = 8\pi p(z), \quad (10)$$

where we have defined a dimensionless  $s$  (positive when pressure falls at greater height) by,

$$s(z) = - \int_z A(z') (dp/dz') dz' / [A(z)p(z)]. \quad (11)$$

Notice that  $s = 0$  for the constant pressure case and that  $(1 - s)/s$  is the constant  $d \ln(A)/d \ln(p)$  when  $A$  the cross sectional area varies as a power of  $p$ .

Two possible approaches to solving this problem are:

#### I. FORWARDS METHOD

We use the energy variational principle choosing such simple trial functions that the boundary conditions can be applied and the resulting variational equations can be solved. We can then solve the problem for all choices of the prescribed functions  $P(R, 0)$ ,  $\Phi(P)$  and  $p(z)$  but the accuracy of the solution is limited by the imposed form of the trial function.

#### II. BACKWARDS METHOD

Here we solve the exact equation (3) but make special choices of  $\beta(P)$  and of the surface  $S$  so that we can solve the problem. Once we have the solution we discover the functions  $P(R, 0)$ ,  $\Phi(P)$ , and  $p(z)$  for which we have the solution. While this method is limited to a very few special cases, at least for them the solutions are exact. This enables us to check the accuracy and the validity of the more general solutions given by the Forwards method.

### 3 SOLUTION BY VARIATIONAL PRINCIPLE

This method was developed in paper III and with an extremely crude but instructive trial function it was used in paper II. There we showed that if each field line turned  $N$  times around the axis and the magnetic cavity was taken as a cylinder of height  $Z$  and radius  $R$  then, if the total uprising poloidal flux was  $F$ , very crude estimates of the field components are:  $B_z = 2F/(\pi R^2)$ ;  $B_R = F/(\sqrt{2}\pi RZ)$ ;  $B_\phi = NF/(RZ)$ . Squaring these estimates, adding the external pressure  $p$  and

multiplying by the volume  $\pi R^2 Z$  we find  $8\pi^2 W = F^2[(1/2 + N^2\pi^2)Z^{-1} + (4R^{-2} + 8\pi^3 p R^2 F^{-2})Z]$  where  $p$  is assumed independent of  $z$ . Minimising over  $R$  gives  $R = (2\pi^3 p/F^2)^{-1/4}$  so  $R$  is determined by the external pressure and the flux. With this result the final round bracket in  $W$  reduces to  $8R^{-2}$  and minimising  $W$  over all  $Z$  we find  $4Z/R = \sqrt{1 + 2N^2\pi^2} \rightarrow \sqrt{2\pi}N$  which shows a remarkable collimation which improves with every turn!

The method of paper III involved a much improved trial function which allows each field line,  $P$ , to attain whatever maximum height,  $Z(P)$  it likes, allows for the different total twists  $\Phi(P)$  of the different field lines and properly accounts for the variation of external pressure with height. Because of the great heights of the magnetic towers generated after many turns, most of the field energy is high above the accretion disk and the detailed distribution of the flux in  $P(R, 0)$  no longer plays a part in the distant field. At each height,  $z$ , mean fields are defined by

$$\overline{B}_\phi(z) = R_m^{-1} \int_0^{R_m} B_\phi(R, z) dR, \quad (12)$$

where  $R_m(z)$  is the radius of the magnetic cavity at height  $z$ , and  $A(z) = \pi R_m^2$ . Also

$$|\overline{B}_z| = A^{-1} \int_0^{R_m} |B_z| 2\pi R dR = A^{-1} \int |\partial P / \partial R| dR = 2P_m/A. \quad (13)$$

The last expression arises because  $P$  is zero at both  $R = 0$  and  $R = R_m$  and achieves its maximum  $P_m(z)$  at an intermediate point. We also define

$$I^2 = \langle B_z^2 \rangle / |\overline{B}_z|^2, \quad (14)$$

and

$$J^2 = \langle B_\phi^2 \rangle / \overline{B}_\phi^2; \quad (15)$$

although  $I$  and  $J$  are in principle functions of height, for tall towers we expect them to settle down to some typical values which we determine later. In what follows we neglect any variation of  $J$  with height; variation of  $I$  does not change the result. We now explain the basis of the trial function used.

If a poloidal flux  $dP$  is twisted once around the axis, it generates a toroidal flux  $dP$ . If its twist is  $\Phi(P)$  the toroidal flux generated is  $(2\pi)^{-1} \Phi(P) dP$ . First consider distributing this toroidal flux uniformly over the height  $Z(P)$  to which this field line reaches as was done in paper III. Unlike the use of  $Z$  in the crude calculation in its new meaning it depends on the  $P$  of the field line. In a small height interval  $dz$  the element of flux  $dP$  contributes a toroidal flux  $[2\pi Z(P)]^{-1} \Phi(P) dP dz$  whenever the height is less than  $Z(P)$ . The total toroidal flux through  $dz$  is contributed by all lines of force that reach above that height; that is by those with  $P < P_m(z)$ , where  $P_m(z)$  is the maximum value that  $P$  achieves at height  $z$ . Hence there is a toroidal flux through the area  $R_m dz$  of

$$R_m \overline{B}_\phi dz = (2\pi)^{-1} \int_0^{P_m} (\Phi/Z) dP dz;$$

$\Phi(P)$  is specified in terms of the accretion disk's twist.  $Z(P)$  is to be varied. However while this makes a possible trial function it is not generally true that the flux is so distributed. Indeed in the limiting case of the exact self-similar solutions discussed in the next paper the twist is strongly concentrated toward the top of each field line. The extreme alternative is found by putting all the twist at the top of each field line. Then the toroidal flux in any height increment  $dz$  depends on the twist of those field lines whose tops lie in  $dz$  so  $R_m \overline{B}_\phi dz = (2\pi)^{-1} \Phi(P_m) (-dP_m/dz) dz$ . However the truth must lie between the extremes of uniform twist and all twist at the top of each line. We therefore take the geometric mean of these two expressions for the toroidal flux distribution and obtain:

$$R_m \overline{B}_\phi = (2\pi)^{-1} [\Phi(P_m) (-dP_m/dz) \int_0^{P_m} (\Phi/Z) dP]^{1/2}. \quad (16)$$

Now  $Z(P)$  is in the variational principle and  $P_m(z)$  has the property that  $P_m[Z(P)] = P$ , so  $P_m$  is the functional inverse of  $Z(P)$ ; so whenever  $Z(P)$  is varied  $P_m(z)$  automatically varies in concert. We now omit the  $B_R^2$  term in the energy principle as it is much smaller than the others once the towers grow tall, cf the crude estimate above equation (12). Writing  $W$  in terms of the expressions discussed above

$$8\pi W = \int \left[ (4\pi)^{-1} J^2 \Phi(P_m) (-dP_m/dz) \int_0^{P_m(z)} \Phi/Z dP + 4I^2 P_m^2/A + 8\pi p(z)A \right] dz \quad (17)$$

Varying  $A(z)$  gives

$$A = \pi R_m^2 = I P_m / \sqrt{2\pi p(z)} \quad (18)$$

which using (13) and (14) is equivalent to  $\langle B_z^2 \rangle = 8\pi p$ , as found in equation (9). Putting this expression back into

equation(17) we find that the last two terms there combine to make  $P_m d\Pi/dz$  where  $\Pi = \int_0^z 4I\sqrt{2\pi p(z')}dz'$ . We now integrate both terms in  $W$  by parts and then rename the dummy variables in the integrals that result from the first term; these operations give

$$8\pi W = (4\pi)^{-1} J^2 \int_0^F [\Phi(P_m)/Z(P_m)] \int_{P_m}^F \Phi(P) dP dP_m + \int_0^F \Pi dP_m, \quad (19)$$

where  $\Pi$  is merely  $\Pi(z)$  re-expressed as a function of  $P_m$

$$\Pi(P_m) = \int_0^{Z(P_m)} 4I\sqrt{8\pi p(z)} dz \quad (20)$$

Most remarkably our adopted geometric mean between the uniform twist and top- twist cases has resulted in a  $W$  of precisely the form obtained in the uniform twist case of paper III except that the first term is now exactly half of its former value. Since this clearly reduces  $W$  the new trial function is clearly better than the old in that it brings us closer to the true minimum. Minimising  $W$  over all choices of  $Z(P_m)$  we find from (19) and (20)

$$Z^2 \sqrt{8\pi p(Z)} = [J^2/(16\pi I)] P_m \bar{\Phi}(P_m)^2 \quad (21)$$

where

$$\bar{\Phi}^2 = \Phi(P_m) P_m^{-1} \int_{P_m}^F \Phi(P) dP \quad (22)$$

Equation (21) gives the function  $Z(P_m)$  and its inverse  $P_m(z)$  in terms of the given  $p(z)$  and  $\Phi(P)$ . In line with section two's introduction we write  $\Phi = \Omega t$  and  $\bar{\Phi} = \bar{\Omega} t$ . From equation (21) we notice that as a result of this  $t$  dependence  $\bar{\Phi}$  and  $Z$  grow with  $t$  at each value of  $P_m$ . This growth is at constant velocity if the external pressure is independent of height. However if that pressure falls off with height the velocity  $dZ/dt$  accelerates. e.g. if  $p \propto (a + Z)^{-n}$  with  $n = 2$  then  $Z$  has nearly constant velocity until it reaches 'a' but at greater heights it behaves as  $t^2$  with constant acceleration. The shape of the magnetic cavity at each moment is given by plotting  $Z$  against  $R_m(Z)$ . We find the relationship by substituting  $P_m$  from equation (18) into equation (21) to give the equation for  $Z$  as a function of  $R_m$ . Viz  $Z = [J/(4\sqrt{2}I)] R_m \bar{\Omega} [\pi I^{-1} R_m^2 \sqrt{2\pi p(Z)}] t$ , where  $\bar{\Omega}$  is evaluated at the value of  $P_m$  indicated in its square bracket. Dividing equation (21) by equation (18) we find the collimation at any given  $P_m$  is just

$$Z/R_m = [J/(4\sqrt{2}I)] \bar{\Omega}(P_m) t, \quad (23)$$

which still grows linearly with time even when the external pressure decreases with height. However  $p(z)$  should not decrease too fast else equation (21) will not have a sensible solution. To understand this we see from equation (22) that  $P_m \bar{\Phi}^2$  decreases as  $P_m$  increases since the twist  $\Phi(P_m)$  is greatest for the field lines rising nearest the centre of the disk. Also  $P_m$  decreases at greater heights since less magnetic flux reaches there. Hence  $P_m \bar{\Phi}^2$  increases with height  $Z$ . This must be true of the left hand side of equation (21) too and indeed it is obviously so when  $p$  is constant so there is then a sensible solution. However should  $p(Z)$  decrease faster than  $Z^{-4}$  the left hand side of (21) would decrease with  $Z$  so there would be no such solution. If the cavity accesses regions in which  $p$  decreases a little less fast than  $z^{-4}$  then the field rapidly expands outwards and this gives a most interesting jet model. For example if  $p \propto (a + z)^{-(4-\delta)}$  then  $Z$  would grow with a very high power of  $t$ ,  $t^{2/\delta}$  at each  $P_m$  so high expansion speeds would be achieved quite soon; however ram pressure will increase the effective pressure at the jet's head. This is explored in a later section. When relativistic speeds are achieved our approximation fails but analytical progress with relativistic jets can now be achieved following the lead of Prendergast (2005). For static pressures with  $p = p_0/[1 + (z/a)]^n$  we illustrate the motion of the jet-head in Figure 1. For  $Z < a$  the velocity is almost constant but as the jet encounters the decrease in pressure it accelerates. For  $n = 2$  the acceleration becomes uniform, but for larger  $n$  it increases and for  $n = 4$  infinite speeds would occur in finite time if our equations still held. For  $n > 4$  the graph turns back so the solutions indicate an infinite speed and then turn back giving no solutions for later times. These results are of course modified when ram-pressure is included as described later.

### 3.1 CAVITY SHAPES FOR SPECIFIC MODELS

We have the solution for any specified distributions of  $p(z)$  and for any twist  $\Phi(P) = \Omega(P)t$ . However before we can draw any cavity shapes we must also specify  $\Omega(P)$  or equivalently  $\bar{\Omega}(P)$ . These two are connected through the definition  $P[\bar{\Omega}(P)]^2 = \Omega(P) \int_P^F \Omega(P') dP' = -(1/2) d/dP [\int_P^F \Omega(P') dP']^2$ . This relationship is easily inverted. Evidently  $\int_P^F \Omega(P') dP' = [\int_P^F 2P\bar{\Omega}^2 dP]^{1/2}$  so finally  $\Omega(P) = P\bar{\Omega}^2 [\int_P^F 2P\bar{\Omega}^2 dP]^{-1/2}$ . We expect the behaviour of  $\Omega(P)$  near  $P = F$  should be proportional to  $(F - P)^2$  since on the disk  $B_z = 0$  there. From the definition above this implies that  $\bar{\Omega}^2$  should be proportional to  $(F - P)^3$  near there. It is also true that if  $\Omega$  tends to  $\Omega_0$  as  $P$  tends to zero then  $\bar{\Omega}$  will be proportional to  $P^{-1/2}$  near there.

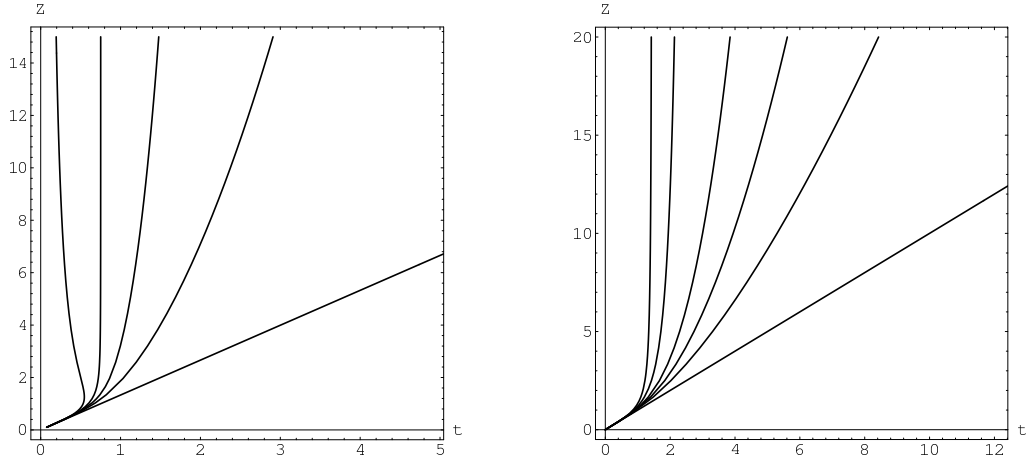


**Figure 1.** Figure 1 shows the time evolution of the height of the jet in different pressure environments. On the left for the lowest graph the jet penetrates a constant pressure environment,  $n=0$ , at constant speed; the higher graphs are for  $n=2,3,4,6$ , and  $n=2$  has almost constant velocity up to  $Z=a$  but feels the pressure decrease and thereafter proceeds at almost constant acceleration. At higher  $n$  the acceleration increases and there are no continuing solutions with magnetic pressure in balance beyond  $n=4$ . In fact the  $n=6$  curve turns back unphysically to earlier times because the external pressure is too weak to withstand the magnetic field at larger heights. In reality the magnetic field springs outward at such a speed that dynamic ram-pressure comes into play. On the right we see the equivalent figure for ram-pressure with density profiles  $m=0,2,3,4,6,8$  see equation (26)

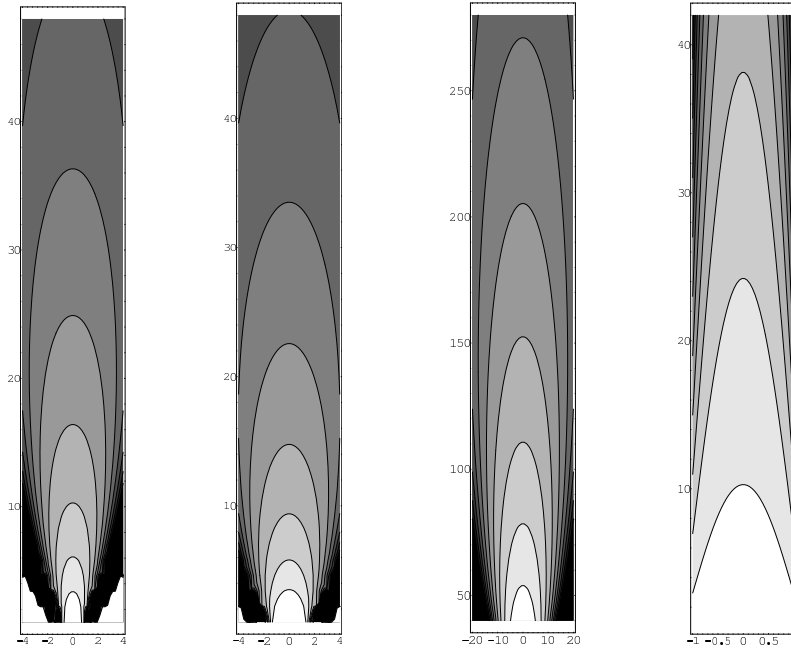


**Figure 2.** The two figures on the left give the temporal evolution of the cavity shapes for the Dipole (left) and Simple models for the  $n=3$  pressure distribution. The times corresponding to a given jet height are given in figure 1. Next we have the Simple model at a later time (notice the scale change). These are contrasted with the evolution of a magnetic cavity in a constant pressure environment  $n=0$ , on the right; here at each time the cross sectional area is always smaller at greater height.



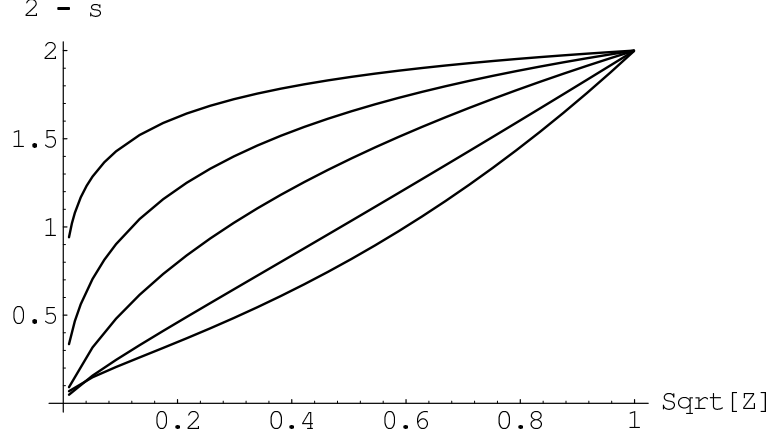


**Figure 3.**  $\langle B_\phi^2 \rangle / \langle B_z^2 \rangle$  plotted as a function of  $\sqrt{z/Z_h}$  for pressure-confined Simple-model jets with from the top  $n=0.2, 0.5, 1, 2, 3$ . Both field components become zero at the jet's head

The simplest expression with these properties is the Simple Model  $\bar{\Omega} = (2)^{-1/2} \Omega_0 (P/F)^{-1/2} (1 - P/F)^{3/2}$ . This steadily falls from its central value and corresponds to  $\Omega(P) = \Omega_0 (1 - P/F)$ .

A model with a more physical motivation is a uniformly magnetised rapidly rotating star or black hole giving an initial flux distribution on the disk  $P(R, 0) = FR^2/a^2$  for  $R < a$  and  $P = Fa/R$  for  $R > a$ . This Dipole Model has a sudden reversal of field at  $R = a$ . We combine this with a rotation  $\Omega_d = \Omega_*$  for  $R < a$ ;  $\Omega_d = \Omega_* (R/a)^{-3/2}$  for  $R > a$ . Setting  $Y = P/F$ ,  $\Omega = \Omega_* [1 - Y^{3/2}]$  and on integration  $\bar{\Omega}(P) = \Omega_* Y^{-1/2} \sqrt{(1 - Y^{3/2})[3/5 - Y + (2/5)Y^{5/2}]}$ .

The shapes of some of the dynamic magnetic cavities generated by combining these  $\Omega(P)$  distributions with simple ambient external pressure distributions  $p(z)$  are illustrated in Figure 2.

Figure 2 shows the time evolution of the magnetic cavity for the  $n = 3$  pressure distribution for the Dipole and the Simple models. They do not differ much. Very different cavities and velocities arise when the pressure distribution in the ambient medium is changed. In particular larger  $n$  albeit less than 4 gives a fatter jet at a given length and a longer jet at a given time as illustrated in figure 2, however the collimation as determined by the length to width ratio is governed by equation (23) and so remains about the same at a given time. With the shapes of the cavities known it is now possible to calculate their areas at each height for each external pressure and thus discover how  $s(z)$  varies with height. This is interesting as, from (10),  $\langle B_\phi^2 \rangle / \langle B_z^2 \rangle = 2 - s$ . For  $z \gg a$  the distribution of  $2 - s$  with  $(z/Z_h)^2$  is given for various values of  $n$  using the Simple Model. These graphs illustrate that the twist is less for the higher values of  $n$  but for them it is more concentrated toward the top of the jets. The integrations for equation (11) were performed by expressing the area as a function of pressure via equations (18), (21) and (23). The final function for  $z \gg a$  which is plotted is  $2 - s = (1/2)[(4 - n)/(n - 1)]x^b[(1 - x^c)/(1 - x^b)]$  where  $x^2 = (z/Z_h)$ ;  $b = (4 - n)/3$ ;  $c = 4(n - 1)/3$

### 3.2 FAST JETS – RAM PRESSURE

Our most suggestive finding thus far is that there are NO quasi-static solutions of large total twist  $\Phi$  when the external pressure falls like  $z^{-4}$  or faster. This result is easily understood; A purely radial field in a bottom-truncated cone  $r > a$  of solid angle  $\omega$  will fall like  $r^{-2}$ . If the total poloidal flux both outwards and inwards is  $F$  the magnetic field would be  $2F/[\omega r^2]$  and it would deliver a pressure  $F^2/[2\pi\omega^2 r^4]$  on the walls. The total field energy would be  $F^2/[2\pi\omega a]$  and an equal amount of work would be needed to inflate the magnetic cavity against the external pressure so the total energy would be  $F^2/[\pi\omega a]$ . If instead we had a pure potential field with the same flux its field would fall as  $r^{-(l+2)}$  so its energy would be about  $F^2/[2\pi(2l + 1)\omega a]$  where  $l$  is the order of the Legendre polynomial that fits into the solid angle; so the energy of the purely radial field to infinity and back is only about  $2l + 1$  times the energy of the potential field. In practice  $l = (4\pi/\omega)^{1/2}$ . In paper V we find that a total twist of the upgoing flux relative to the downcoming flux, of  $\pi/\sin[\theta_m/2]$  is sufficient for the flux to extend to infinity within a cone of semi-angle  $\theta_m$ . When the pressure falls with a power a little less negative than minus four we already demonstrated that continued twisting leads to the top of the tower or jet head advancing with a very high power of the time. However that was on the basis of a static pressure which will be enhanced by the dynamic ram-pressure once speeds comparable with the sound speed are achieved. Applying Bernoulli's equation in the frame with the jet-head at rest we have  $v^2/2 + [\gamma/(\gamma - 1)]p/\rho = \text{constant}$ , so at the stagnation point  $p_s = p[1 + (\gamma - 1)/2\gamma\rho v^2/p]^{\gamma/(\gamma - 1)}$ . If  $p \gg \rho v^2$  we

get  $p_s = p + \rho v^2/2$ . Although that is much used we are more interested in the general case. When the flow becomes supersonic a stand-off shock develops so the above formula needs to be modified. Just behind the bow shock the pressure and density are given in terms of the upstream Mach number  $M$  by  $p_2 = p(\gamma + 1)^{-1}[2\gamma M^2 - (\gamma - 1)]$ ;  $\rho_2 = \rho(\gamma + 1)M^2/[(\gamma - 1)M^2 + 2]$ ; also  $\rho_2 v_2 = \rho v$ . Applying Bernoulli's theorem after the shock results in a formula which for Mach numbers of two or more is well approximated by  $p_s = \Gamma(\gamma)\rho v^2$ . Here  $\Gamma = [(\gamma + 1)/2]^{(\gamma+1)/(\gamma-1)}\gamma^{-\gamma/(\gamma-1)}$  which is 1, 0.93, 0.88 for  $\gamma = 1, 4/3, 5/3$ , respectively. The full formula for  $p_s$  has a further factor on the right  $[1 - (\gamma - 1)/(2\gamma M^2)]^{-1/(\gamma-1)}$  which clearly tends to one at large  $M^2$ . For  $\gamma = 4/3$  it ranges between 1.49 --  $> 1.05$  as  $M$  ranges from one to three. For  $\gamma = 5/3$  the range is from 1.41 --  $> 1.03$ . A useful global formula that somewhat approximates the trans-sonic pressure but is good in both the static and strongly supersonic limits is

$$p_s = p + \rho v^2. \quad (24)$$

This is the stagnation pressure that will be felt at the head of the jet. Away from the head the pressure is reduced both because the magnetic cavity expands less rapidly in the direction of its normal there and because a considerable fraction of the velocity is now parallel to the surface of the cavity. We return to this in the paragraph on Inertially Confined Jets.

### 3.3 MOTION OF THE JET-HEAD

From equations (21) & (22) the position of the jet head at time  $T$  is  $Z_h$  where

$$Z_h^2 \sqrt{8\pi p_s} = J^2 [16\pi I]^{-1} \Omega(0) \int_0^F \Omega(P) dP \cdot t^2 \quad (25)$$

where, because we are dealing with the head, we have replaced the pressure with the stagnation pressure and set  $P_m = 0$ . With the stagnation pressure given by (24) but  $\dot{Z}_h$  replacing  $v$ , equation (25) is now an equation of motion for the jet-head. As only  $Z_h$  occurs in this subsection we shall usually drop the suffix  $h$  which will be understood. When formulae are to be used in other sections we shall resurrect the suffix so that they can be lifted unchanged. Squaring (21)  $p(Z) + \rho(Z)\dot{Z}^2 = L^2(t/Z)^4$  where  $p(z)$  and  $\rho(z)$  are the undisturbed pressure and density at height  $z$  and  $L$  is the constant  $(1/2)(8\pi)^{-3/2} J^2 I^{-1} \Omega(0) \int_0^F \Omega(P) dP$ . We are interested in this equation when pressure falls with height. If the initial velocity given by neglecting the  $\dot{Z}^2$  term is subsonic then initially we shall have results very similar to the quasi-static case illustrated on the left of figure 1 but all those solutions accelerate as the pressure decreases so the velocity will become sonic and then supersonic so that the  $\rho(Z)\dot{Z}^2$  term will dominate over the falling pressure. Now neglecting the pressure and taking the square root we have  $Z^2[\rho(Z)]^{1/2}\dot{Z} = Lt^2$ . Setting

$$\rho(Z) = \rho_0[1 + (Z/a)^3]^{-m/3}, \quad (26)$$

so that the density behaves as  $z^{-m}$  at large heights, we integrate to find

$$[1 + (Z/a)^3]^{1-m/6} - 1 = (1 - m/6)L_1 t^3. \quad (27)$$

where  $L_1 = L\rho_0^{-1/2}a^{-3}$ . For all  $m$  the solutions for small heights are  $Z = a(L_1)^{1/3}t$  and for large heights

$$Z_h = a[(1 - m/6)L_1]^{2/(6-m)} t^{6/(6-m)} \dots m < 6. \quad (28)$$

Once again such solutions accelerate but less rapidly; however if the density ever falls as fast as height to the minus six even the ram-pressure is too weak and the solutions rise formally to infinite speed before failing altogether when  $t = [6/(m - 6)]^{1/3} F^{1/6} L_1^{-1/3}$ . The trouble arises because the rapid fall in density gives too small a ram-pressure to resist the acceleration of the jet. In practice either the excess inertia due to relativistic motion or the fact that the density does not fall below intergalactic values will avoid this behaviour. In the former case we need to develop the relativistic MHD jet theory. In the latter we may use our  $m < 6$  model modified by replacing the density by the intergalactic one whenever our formula yields a smaller value, i.e. at  $Z_h > a[(\rho_0/\rho_i)^{3/m} - 1]^{1/3}$ . As it reaches this region the velocity reaches  $\dot{Z}_h = [L(\rho_i)^{-1/2}]^{1/3}$  and thereafter it remains at that value. So  $Z_h(t)$  is given by formula (28) displayed in Figure 1 (right) until it reaches that region but then maintains its constant speed.

### 3.4 INERTIALLY CONFINED SUPERSONIC JETS

Landau and Lifshitz in their Fluid Mechanics book paragraph 115 give an elegant theory of supersonic flow past a pointed body, and the pressure on the body may be found by using the stress tensor  $\rho(\partial\phi/\partial R)^2$  of the velocity potential given in their formula 115.3. However there are two drawbacks. Firstly it is not likely that our jet will constitute a pointed body rather than a blunt one, even if it could be treated as a body at all, and secondly the resulting formulae involve integrals over the shape of the body which we can only discover AFTER the pressure is known. We shall circumvent such difficulties while maintaining momentum balance by treating the medium into which the jet penetrates as ionised dust each particle of which

collides with the magnetic cavity. Taking axes that move with the top of the field lines labelled by  $P$  i.e. with velocity  $\dot{Z}(P)$  we find a ram-pressure on the cavity wall at height  $Z$  of  $2\rho\dot{Z}^2\cos^2\theta$  where  $\cos^2\theta = \frac{1}{[1+(\partial Z/\partial R)_t^2]}$ . The factor two arises from the assumption of specular reflection from the cavity wall and at normal incidence the formula gives a factor two more than the stagnation pressure at the jet head. This suggests that a dead-cat-bounce off the cavity wall may be a better approximation than a specular reflection so we shall omit the factor two in what follows. However even the resulting formula is hard to apply in practice so we now proceed to simplify it further. Most of our jets are not far from parabolic at the front, in which case  $Z_h - Z = \kappa(t)R_m^2$ . Then  $(\partial Z/\partial R_m)^2 = 4(Z_h - Z)^2/R_m^2$ . Hence we shall adopt for the dynamic pressure at  $Z(P)$

$$p_d = \rho\dot{Z}(P)^2/[1 + 4(Z_h - Z)^2/R_m^2] \quad (29)$$

To find the shape of a dynamically confined jet we need to solve equation (21) with the dynamic pressure  $p_d$  replacing  $p$  and use equations (23) and (26) for  $R_m$  and  $\rho(z)$ . For  $Z \gg a$  equation (21) becomes

$$Z^{2-m/2}\dot{Z}\sqrt{8\pi\rho_0 a^m/[1 + 4(Z_h - Z)^2/R_m^2]} = [J^2/(16\pi I)]P_m\bar{\Omega}^2 t^2. \quad (30)$$

Except near the jet-head  $Z_h - Z \gg R_m/2$  so we may neglect the one and using (23) for  $R_m$  the above equation simplifies to

$$Z^{3-m/2}\dot{Z} = K_1\bar{\Omega}^3 t^3 (Z_h - Z). \quad (31)$$

For an initial orientation we take  $Z_h \gg Z$ . We may then integrate directly using our former result that  $Z_h \propto t^{1/(1-m/6)}$  and obtain  $Z \propto t^{(5-2m/3)/[(1-m/6)(4-m/2)]}$ , whence it follows that  $Z$  grows with a higher power of  $t$  than  $Z_h$  (at least for  $Z$  small) indeed  $X = Z/Z_h \propto t^{1/(4-m/2)}$ . When  $Z$  is sizeable the above overestimates  $\dot{Z}$  so it overestimates  $d\ln X/d\ln t$  which must in reality lie between zero and  $(4-m/2)^{-1}$  which is itself less than  $(1/4)(1-m/6)^{-1}$ . We get a better estimate of the behaviour of  $X$  by writing equation (31) in the form

$$X^{4-m/2}[(1-m/6)(1-X)]^{-1}[1 + (1-m/6)d\ln X/d\ln t] = K_2 t, \quad (32)$$

where at given  $P$ ,  $K_2$  is constant. Now the second square bracket above only varies between one and  $5/4$ . If at lowest order we neglect its variation, we may solve for  $t(X)$ . We may then evaluate

$$d\ln X/d\ln t = (1-X)/[4(1-m/8)(1-X) + X], \quad (33)$$

(32) then determines  $t$  as a function of  $X$ . Evidently the  $t^{1/(4-m/2)}$  behaviour of  $X$  persists approximately until  $X$  is near unity; however  $Z_h - Z \propto t^{1/(1-m/6)}(1-X)$  and this actually grows because with  $X$  near unity the second square bracket in equation (32) is one and so  $Z_h - Z \propto [K_2(1-m/6)]^{-1/(1-m/6)}X^{(4-m/2)/(1-m/6)}(1-X)^{-m/(6-m)}$ , so as  $X$  grows  $Z_h - Z$ , the distance from the head actually increases.  $Z$  never catches up with  $Z_h$  despite the fact that  $X$  tends to one. All the above rests on the premise that  $Z_h - Z \gg R_m/2$  so we now investigate the behaviour when  $Z$  is close to  $Z_h$  so that  $X$  is close to one but not so close that  $(1-X)Z/R_m$  has to be small. Writing equation (30) in terms of  $X$ , but omitting the  $d\ln X/d\ln t$  term as this vanishes with  $X$  near unity, and dividing it by the same equation for  $Z_h$  we find  $1 + 4(Z_h - Z)^2/R_m^2 = X^{6-m}/[K_4(P_m)]^2$  where  $K_4$  is  $P_m\bar{\Omega}^2(P_m)$  divided by its non-zero value when  $P_m$  tends to zero. At constant  $P_m$ ,  $(Z_h - Z)/R_m$  clearly increases as  $X$  increases but it tends to the limiting value  $(1/2)\sqrt{K_4^{-2} - 1}$  as  $X$  tends to one. As  $K_4$  depends only on  $P_m$  the shape of the jet-head is determined by the  $\bar{\Omega}(P)$  function though its size and position depend on  $t$  also. Thus the whole head of the jet and all parts with  $X$  near one grow self similarly. The shape of these parts is even independent of the details of the density fall-off embodied in  $m$  but the size of these parts of the jet is proportional to  $t^{m/(6-m)}$  so the rate of self-similar growth depends on  $m$ . As explained above the whole length of the jet grows with a different power of the time so it is just the part with  $X$  close to one that grows self-similarly. To find the shape of the whole cavity we notice that elimination of Omega-bar between equations (23) and (30) or (21) coupled with use of (33) leads to an expression for  $P_m$  in terms of  $Z, Z_h, R_m, t$

$$P_m = \frac{\pi}{2I(1-\frac{m}{6})}(R_m^2 Z/t) \left[ 1 + \frac{(1-m/6)(1-Z/Z_h)}{[4(1-m/8)(1-Z/Z_h) + Z/Z_h]} \right] \sqrt{\frac{8\pi\rho_0 a^m (Z^3 + a^3)^{-m/3}}{[1 + 4(Z_h - Z)^2/R_m^2]}} \quad (34)$$

This value of  $P_m$  is substituted into the Omega-bar of equation (23) to yield the equation relating  $Z$  and  $R_m$  at each time,  $Z_h(t)$  being already known. Thus we get the shapes of the inertially confined jet cavities. Figure 4 displays one of these at two different times.

#### 4 THE FIELD IN THE MAGNETIC CAVITY

Our solution of the variational principle has improved on paper III and given us dynamical solutions for the cavity's shape and the mean field at each height. We now seek the detailed field structure within the cavity. At each height  $z$  we define  $\lambda$  to be  $[R/R_m(z)]^2$  so  $P$  may then be written

$$P(R, z) = P_m(z)f(\lambda). \quad (35)$$

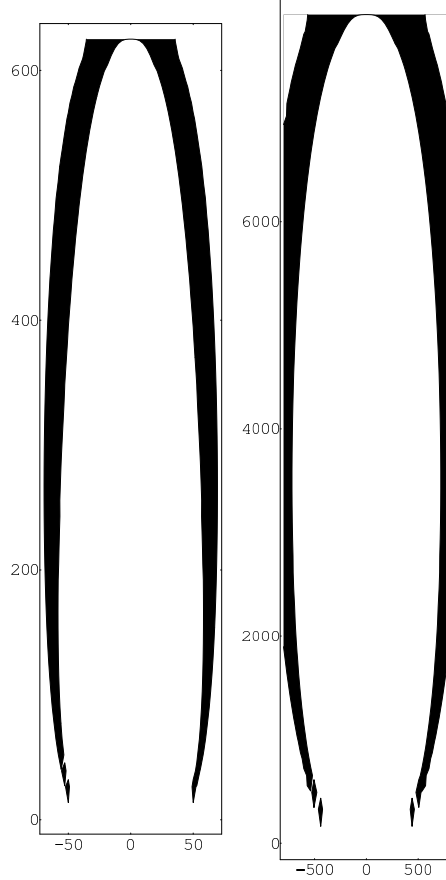


**Figure 4.** An inertially confined jet cavity at two different times, the inner edge of the black gives the cavity in an  $m=3$  density distribution for the Simple model magnetic flux. The times to these heights are given by equation (27)

Since by its definition  $P_m(z)$  is the maximum value that  $P$  takes at height  $z$ , it follows that  $f$  achieves its maximum of unity at each height. Furthermore, as  $P$  is zero both on axis and at the surface of the magnetic cavity, it follows that  $f(0) = 0 = f(1)$ . Thus  $f$ , which is positive, is highly circumscribed rising from zero to one and falling again to zero at one. Although  $f$  may in principle depend on height (especially near the disk or at the top), nevertheless so circumscribed a function is unlikely to have a strong height dependence. We shall make a second approximation that an average profile will do well enough over at least a local region of the tower's height. Thus we adopt the form given in equation (35) with  $f$  a function of  $\lambda$  but not of height. Now in the tall tower limit both  $R_m(z)$  and  $P_m(z)$  are only weakly dependent on  $z$ , so squares of their first derivatives and their second derivatives may be neglected. Equation (3) then takes the form

$$4P_m R_m^{-2} \lambda \partial^2 f / \partial \lambda^2 = -\beta \partial \beta / \partial P = -(\partial \beta^2 / \partial \lambda) / (2P_m f'). \quad (36)$$

Multiplying by  $2P_m f'$  and integrating  $d\lambda$  we find  $\beta^2 = 4P_m^2 R_m^{-2} (\int_0^\lambda f'^2 d\lambda - \lambda f'^2)$ , so  $\beta(P)$  is of the form  $\beta[P_m f(\lambda)] = (2P_m/R_m)G(\lambda)$ . Evidently  $\beta$  is a product of a function of  $z$  and a function of  $\lambda$  but it is also a function of such a product. It is readily seen that a power law form for  $\beta$  achieves this and we readily prove that the power law is the only possibility that allows it. Hence we may write

$$\beta = C_1 P^\nu. \quad (37)$$

Thus  $\beta' / \beta \propto \nu P^{2\nu-1}$ . Inserting this into equation (36) and calling the value of  $\lambda$  where  $f$  achieves its maximum of one,  $\lambda_1$ , we find on separating the variables  $\lambda$  and  $z$  both

$$\lambda d^2 f / d\lambda^2 = -C^2 \nu f^{2\nu-1}, \quad (38)$$

and

$$R_m = C_2 P_m^{1-\nu}, \quad (39)$$

where

$$C^2 = C_1^2 C_2^2 / 4. \quad (40)$$

Now  $P_m(z)$  decreases because not all flux reaches up to great heights, so equation (39) tells us that the radius of the magnetic cavity decreases there when  $\nu < 1$  and increases when  $\nu > 1$ . Of course this only holds once the tower is tall so that its lateral confinement is due to the ambient pressure rather than the flux profile on the disk itself. The constant  $C$  is determined by the requirement that  $f = 1$  at its maximum because  $f(\lambda)$  already has to obey the boundary conditions at 0 and 1. Sometimes we find it convenient to use  $\alpha = 2\nu - 1$  in place of  $\nu$ . We already know how to calculate the shape of the magnetic cavity. Knowing  $A(z)$  and  $p(z)$  we can calculate  $s = -(Ap)^{-1} \int_z A(z') (dp/dz') dz'$  at every height  $z$ . We now show that associated with each value of  $s$  there is a profile  $f(\lambda)$ . Equation (38) governs the possible profiles. Multiplying it by  $-f/\lambda$  and integrating by parts we find  $\int_0^1 (f')^2 d\lambda = C^2 \nu \int_0^1 f^{2\nu} \lambda^{-1} d\lambda$ . However  $P_m f' = A(2\pi R)^{-1} \partial P / \partial R = AB_z$  so the first integral is related to  $\langle B_z^2 \rangle$  and the right hand one is similarly related to  $\langle B_\phi^2 \rangle$ . Multiplying both sides by  $P_m^2 / A^2$  we find

$$\langle B_z^2 \rangle = \nu \langle B_\phi^2 \rangle \quad (41)$$

so comparing this with equation (10) we find  $s = (2\nu - 1)/\nu$ , so

$$\nu = 1/(2 - s). \quad (42)$$

Thus for each height we have an  $s$  and hence a  $\nu$  for that height and the associated profile is given by solving equation (38) with  $f = 0$  at  $\lambda = 0$  and  $\lambda = 1$  and the value of  $C$  is determined by the condition that  $f$  is one at its maximum. Notice that by this means we have determined the weak variation of the profile with height (see Figure 3).

#### 4.1 PROFILE FOR CONSTANT EXTERNAL PRESSURE

From equations (18) and (39) constant  $p$  corresponds to  $\nu = 1/2$ ,  $\alpha = 0$ , a case of great simplicity. Integrating equation (38) with the boundary conditions that  $f = 0$  at zero and one, we find  $f' = -C^2(1/2)\ln(\lambda/\lambda_1)$  and  $f = -C^2(1/2)\lambda\ln\lambda$  with  $\lambda_1 = 1/e$ . The requirement that  $f = 1$  at maximum then gives  $C^2 = 2e$  so

$$f = -e\lambda\ln\lambda. \quad (43)$$

With  $f$  known we may now evaluate the dimensionless integrals  $I$  and  $J$ ,

$$I^2 = \langle B_z^2 \rangle / \overline{|B_z|^2} = (1/4) \int_0^1 (df/d\lambda)^2 d\lambda = e^2/4, \text{ hence}$$

$$I = e/2 = 1.359. \quad (44)$$

Likewise

$$J = 2 \sqrt{\frac{\int_0^1 (f/\lambda) d\lambda}{\int_0^1 (f^{1/2}/\lambda) d\lambda}} = \sqrt{2/\pi} = 0.798. \quad (45)$$

Thus once we specify  $\Omega(P)$  and  $p$ , our solution for the shape of the magnetic cavity  $R_m(z)$  is known via equations (21), (22), and (23), and within that cavity the structure of the field is given via the poloidal and toroidal flux functions  $P$  and  $\beta$ .

$$P = P_m(z) e\lambda \ln(1/\lambda) \quad (46)$$

$$\beta(P) = 4(2\pi^3 p)^{1/4} P^{1/2} \quad (47)$$

The magnetic fields are given by  $B_R = -(2\pi R)^{-1} \partial P / \partial z$ ,  $B_\phi = (2\pi R)^{-1} \beta$ ,  $B_z = (2\pi R)^{-1} \partial P / \partial R$ . These are surprisingly interesting,

$$B_z = \frac{1}{\pi R_m^2} \frac{\partial P}{\partial \lambda} = \frac{e P_m(z)}{\pi R_m^2} [\ln(1/\lambda) - 1], \quad (48)$$

which is positive for  $\lambda < 1/e$ , zero at  $\lambda = 1/e$ , and negative for  $\lambda > 1/e$  reaching the value  $-e P_m / (\pi R_m^2)$  at the boundary  $\lambda = 1$ . By equation (18) the magnetic pressure precisely balances the external pressure there. Unexpectedly we find that  $B_z$  is infinite on the axis

$$B_z \propto \ln(R_m/R), \quad (49)$$

however the flux near the axis is small because  $P$  behaves like  $R^2 \ln(R_m/R)$  there. Likewise the contribution to the energy from the magnetic energy-density near the axis behaves as  $R^2 [\ln(R_m/R)]^2$  so the infinity in the magnetic field appears to be harmless. A greater surprise comes from the behaviour of  $B_\phi$  near the axis.

$$B_\phi = \frac{2eP_m}{\pi R_m^2} \sqrt{\ln(R_m/R)}, \quad (50)$$

whereas we expected to find  $B_\phi$  to be zero on axis, it is actually infinite! However the ratio

$$B_\phi/B_z \rightarrow [\ln(R_m^2/R^2)]^{-1/2} \rightarrow 0 \quad (51)$$

thus although the field lines near the axis do wind around it helically, the helix gets more and more elongated as the axis is approached so the axis itself is a line of force. Faced with this example it is evident that the normal boundary condition that on axis  $B_\phi$  should be zero should be replaced by the condition that  $B_\phi/B_z$  should be zero on axis. Since the field is force-free the currents flow along the field lines and  $4\pi\mathbf{j} = \beta'(P)\mathbf{B} = (C_1/2)P^{-1/2}\mathbf{B}$ . As  $P$  is zero on axis  $\mathbf{j}$  is even more singular on axis than the magnetic field. Nevertheless the total current parallel to the axis and crossing any small area is finite and tends to zero as the area shrinks onto the axis. The exact Duncce's Cap model of section 6 gives the same field structure close to the axis. In the next section we find that the infinite fields on axis are replaced by large finite ones when the pressure decreases at greater heights. Current sheets are of course a common feature of idealised MHD and we have one of necessity on the boundary of the magnetic cavity. The infinite field strengths and current densities on axis encountered in this solution suggest that very large current densities occur close to the axis in reality. The lack of sufficient charge carriers there will lead to a breakdown of the perfect conductivity approximation with large EMFs appearing up the axis resulting in particle acceleration along the axis. What observers 'see' as a jet may be just this very high current-density region where the particles are accelerated, i.e. only the central column of the whole magnetic cavity which may be considerably wider, cf the observations of Hercules A, Gizani & Leahy (2003).

## 4.2 PROFILES WHEN PRESSURE DECREASES WITH HEIGHT

Even when the pressure varies we know how to calculate the shape of the magnetic cavity, so all we need is the profile of the field across the cavity. So we need to solve equation (38). For  $\nu = 1/2$  equation (43) gives the solution, but we need it for more general  $\nu$ . While this is easily computed an analytical approximation is more useful. For  $\nu < 1$  a good approximation is given by noting that for  $\alpha = 2\nu - 1$  small  $-\ln \lambda \approx (1 - \lambda^\alpha)/\alpha$ ; using this in our  $\alpha = 0$  solution for  $f$  suggests the form  $f \propto \lambda(1 - \lambda^\alpha)/\alpha$  but a better approximation is given by  $f = g(\lambda)/g(\lambda_1)$  where

$$g(\lambda) = \alpha^{-1} \lambda(1 - \lambda^\alpha)/(1 + a_2 \lambda^\alpha), \quad (52)$$

and  $\lambda_1$  is given by  $g'(\lambda_1) = 0$ . Notice that the denominator in  $g$  is constant when  $\alpha = 0$  so it makes no difference to that solution. This form for  $f$  automatically satisfies both the boundary conditions and the one-at-maximum condition. The equation that gives  $\lambda_1$  is a quadratic in  $\lambda_1^\alpha$

$$1 - [\alpha + 1 - a_2(1 - \alpha)]\lambda_1^\alpha - a_2\lambda_1^{2\alpha} = 0. \quad (53)$$

We use it to find  $a_2$  in terms of  $\lambda_1$  which we determine below

$$a_2 = [1 - \lambda_1^\alpha(1 + \alpha)]/[\lambda_1^\alpha[1 - (1 - \alpha)\lambda_1^\alpha]]. \quad (54)$$

The logarithmic infinities in the fields on axis found in equations (48)-(50) occur because of the log term in equation (46). The form of equation (52) shows that large finite fields replace those infinities when  $\alpha > 0$  and so  $B_\phi \rightarrow 0$  on axis.

For  $\alpha = 1$  there is another exact solution in terms of the Bessel function  $J_1$ ,

$$f = k_1 \sqrt{\lambda} J_1(k_1 \sqrt{\lambda})/[k_0 J_1(k_0)]; \quad (55)$$

here  $k_0 = 2.405$  is the first zero of the Bessel function  $J_0$  and  $k_1 = 3.832$  is the first zero of  $J_1$ . The value of  $\lambda_1$  is therefore  $[2.405/3.832]^2 = 0.3939$ . This is not too far from the value  $1/e = 0.3679$  obtained for our  $\alpha = 0$  solution. This suggests that linear interpolation i.e.  $\lambda_1 = e^{-1}(1 + 0.07073\alpha)$  and  $a_2$  determined via equation (53) will give a good fit and indeed numerical computations show the fit is excellent all the way from 0 to 1, the Bessel case. In the latter the expression  $k_0 J_1(k_0) = 1.249$ .

The integrals  $I$  and  $J$  can be evaluated for the Bessel solutions and we give their values for the  $\alpha = 0$  case in brackets for comparison.  $I = 1.179(1.359)$ ;  $J = 1.098(0.799)$ . As expected  $I$  and  $J$  do change with  $\alpha$  but remain within 15% of their means.

Solutions to equation (38) for large  $\alpha = 2\nu - 1$  were used in paper I to solve a different problem but that method works well and can be extended to work for all  $\alpha$  above unity. Approximate solutions for large  $\nu$  of the form  $f = 1 - \nu^{-1} \ln(\cosh \Lambda)$  where  $\Lambda = 2\Lambda_1(\lambda - \lambda_1) - \Delta \ln(\cosh[\nu C(\lambda - \lambda_1)])$  with  $\Delta = (6\Lambda_1)^{-1}$ ;  $\Lambda_1 = ch^{-1}e^\nu \simeq \nu$ ;  $C \simeq 2\lambda_1^{1/2}$ ;  $\lambda_1 \simeq \frac{1}{2}$  are deduced in the appendix as well as the generalised form

$$f = 1 - H^{-1} \ln(\cosh \Lambda); \dots; \Lambda = C_*(\lambda - \lambda_1) - \Delta \ln(\cosh \Lambda), \quad (56)$$

with  $H = \nu - 1/42 - 5/26.\nu^{-1}$ ;  $h = \sqrt{H\nu}$ ;  $\Delta = 1/2.\nu^{-1} - 1/9.\nu^{-2} + 1/12.\nu^{-3}$ ;  $\lambda_1 = 1/2 - 7/31.\nu^{-1} + 4/41.\nu^{-2}$  and  $C_* = hC\lambda_1^{-1/2} = 2\nu + \ln 4 - 4/15.\nu^{-1}$ . Notice that with  $\Delta$  small equation (56) with  $H = \nu$ ,  $C\lambda_1^{-1/2}$  reduces to

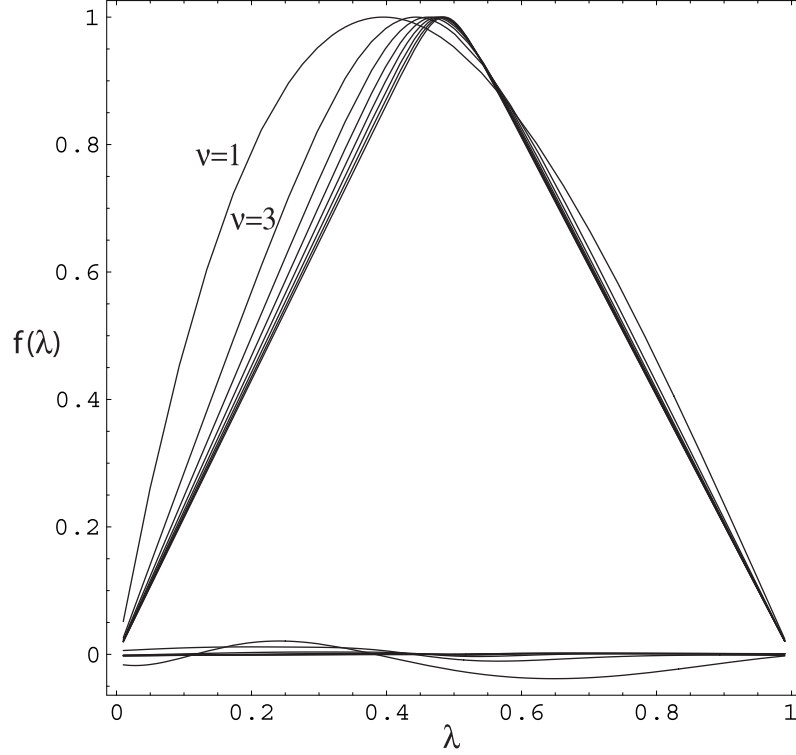


**Figure 5.** Computed profiles  $f(\lambda)$  are plotted for  $\nu = 1, 3, 5, \dots$ . A triangle is the limit  $\nu \rightarrow \infty$ . At the bottom are plotted the errors in our analytic approximate solutions derived in the appendix. Only for  $\nu = 1$  do the errors rise above 2% and for  $\nu = 1$  itself we have the exact Bessel solution.

our former solution. Inclusion of the  $\Delta$  term allows for the asymmetry around the maximum caused by the variation of the initial  $\lambda$  in equation (38). These freedoms allow us to fit exactly, not only the curvature at the maximum and the boundary conditions, but also the gradients at which the solution reaches zero at the ends of the range. Some details are given in the Appendix. The solutions for  $f$  are plotted in Figure 5. By taking  $\nu$  to be given by equation (42) in terms of  $s(z)$  we now have a solution of the form  $P = P_m f(\lambda, \nu)$  with  $\lambda = (R/R_m)^2$  and  $P_m, R_m$  and  $\nu$  all depending weakly on  $z$ , see equations (18), (21) and (42). With  $P$  so determined the function  $\beta(P)$  is found from  $\Phi(P)$  by integrating along field lines. These are given by  $\frac{dR}{B_R} = \frac{Rd\phi}{B_\phi} = \frac{dz}{B_z}$ . Hence

$$\frac{dR}{-\partial P / \partial z} = \frac{Rd\phi}{\beta(P)} = \frac{dz}{\partial P / \partial R} \quad (57)$$

The equality of the first and last terms merely tells us that  $P$  is constant along field lines. The equality of the second and last terms gives us on integration with  $P$  held fixed

$$\beta(P) = \frac{2P\Phi(P)}{\int (d \ln f / d \ln \lambda)^{-1} dz}, \quad (58)$$

where the integration is along the curve  $P$  constant from one foot point to the other. While the above procedure is the one to use when  $P(R, 0)$ ,  $\Phi(P)$  and  $p(z)$  are specified there are special cases that are simpler. If we ask that  $f$  be strictly independent of  $z$  rather than that being an approximation, then equation (39) must hold exactly. Combining that with equation (18) we would have  $p = I^2 (2\pi)^{-1} (\pi C_2 A^{-\alpha})^{-2/(1-\alpha)} \propto P_m^{2\alpha}$ ; from (11) this formula leads directly to  $s = 2\alpha/(\alpha + 1)$  and equation (37) gives us the simple relationship  $\beta(P) = C_1 P^{(\alpha+1)/2}$  in place of equation (58), nevertheless these equations with  $s$  constant imply that  $p$  vanishes, or becomes infinite, when the area  $A$  vanishes, which will not be true. The exactly separable case is too restrictive near the top when the pressure varies.

## 5 ELECTRIC FIELDS, PUSHERS, FLOATERS AND SQUIRMERS

We now determine the electric fields that occur when the accretion disk is in differential rotation. The velocity  $\mathbf{u}$  of a magnetic field line is  $c\mathbf{E} \times \mathbf{B}/B^2$  and there is no  $\mathbf{E}$  along  $\mathbf{B}$  because of the perfect conductivity, hence  $\mathbf{E} = -\mathbf{u} \times \mathbf{B}/c$ . To use this formula we first calculate the velocity of our field lines. On the accretion disk this velocity is that of the disk itself so the field line which initially intersected the disk at azimuth  $\psi$  now has its outer intersection at  $R_o(P)$  at azimuth  $\phi_d = \psi + \Omega_d(R_o)t$ .

We now look for the angular velocity of the point at which this field line intersects a  $z = \text{const}$  plane. At each instant the field line obeys equation (57) so on integrating the second equality there

$$\phi = \psi + \Omega_d(R_o)t + \Omega(P)tq(z.P) \quad (59)$$

where we have written  $\Omega(P)t$  for  $\Phi(P)$  and  $q = \int_0^z (d \ln f / d \ln \lambda)^{-1} dz / \int (d \ln f / d \ln \lambda)^{-1} dz$ . Both integrations  $dz$  are to be performed with  $\lambda$  varying so as to keep  $P$  constant. The final integral is to be performed from foot-point to foot-point. The physical meaning of  $q$  is the fraction of the total twist on the field line  $P$  that occurs by height  $z$ . Since the field line reaches a maximum height  $Z(P)$  and then returns,  $q$  will be double valued as a function of  $z$ . To avoid this it is better to convert those  $z$ -integrations into integrations over  $\lambda$ , in which  $q$  is single valued, rather than  $z$ . Such a conversion yields  $q = \int_{\lambda}^{\lambda_o} Z'(P/f)(f\lambda)^{-1} d\lambda / \int_{\lambda_i}^{\lambda_o} Z'(P/f)(f\lambda)^{-1} d\lambda$ , where we have written  $P/f$  for  $P_m$  to demonstrate that the  $\lambda$  dependence arises through  $f$  when  $P$  is held fixed. The angular rotation rate of the intersection of this field line with a  $z = \text{const}$  plane is

$$\dot{\phi} = \Omega_d + \Omega(P)q + \Omega(P)t\dot{q} \quad (60)$$

$\dot{q}$  arises from two causes i) any explicit dependence of  $Z'$  on  $t$  that does not cancel between numerator and denominator in  $q$ , ii) the change in the lower end point  $\lambda$  of the numerator's integration. At constant  $P$  and  $z$  we have  $\partial \ln P_m / \partial t = -(d \ln f / d \lambda) \dot{\lambda}$ , which gives us the rate of change of the lower limit of the numerator. When  $P(z)$  is either a power or constant the explicit dependence of  $Z'$  on  $t$  cancels between numerator and denominator so there is then no contribution from i). Of course had we left  $q$  as a  $z$ -integration there would have been no contribution from the end point but then the contribution from the  $t$ -dependence of the  $\lambda$  in the integrand must be re-expressed as a function of  $P$  and  $z$  via  $f(\lambda) = P/P_m(z, t)$ , is unwieldy. Now  $R\dot{\phi}$  at constant  $z$  is not the  $\phi$ -component of the velocity of the line of force but the velocity of the point of intersection of the line with the  $z = \text{const}$  plane. When the line of force is only slightly inclined to the plane the difference is obvious since the velocity of the line is perpendicular to the line. A little thought shows that in the intersection velocity the component of the velocity of the line in the  $z$ -plane parallel to the projection of the field into the plane is exaggerated by the factor  $B^2/B_z^2$  relative to that component of the field line's velocity. Thus writing hats for unit vectors and  $\hat{\mathbf{b}}$  for the unit vector  $(B_R \hat{\mathbf{R}} + B_\phi \hat{\phi}) / \sqrt{B_R^2 + B_\phi^2}$  in the  $z$ -plane considered and  $\mathbf{u}_\perp$  for the component of the field line's velocity in that plane, the velocity of the intersection is  $\mathbf{u}_\perp + [(B^2/B_z^2) - 1](\mathbf{u}_\perp \cdot \hat{\mathbf{b}})\hat{\mathbf{b}}$ . The component of this intersection's velocity along  $\hat{\phi}$  is

$$R\dot{\phi} = u_\phi(1 + B_\phi^2/B_z^2) + u_R(B_R B_\phi / B_z^2). \quad (61)$$

Now by Faraday's law, the rate of change of the magnetic flux through a circle about the axis in the plane considered gives the EMF so

$$2\pi R E_\phi = -\partial P / \partial ct = -\dot{P}/c = -(u_z B_R - u_R B_z)/c \quad (62)$$

This is a second equation for  $\mathbf{u}$  and the third is just  $\mathbf{u} \cdot \mathbf{B} = 0$ . Eliminating first  $u_z$  and then  $u_R$  we find  $u_\phi = [(B_R^2 + B_z^2)/B^2]R\dot{\phi} + [B_R B_\phi / (B^2 B_z)]\dot{P}$ . The other components are readily found from equations (61) & (62). The remaining components of  $\mathbf{E}$  follow from  $c\mathbf{E} = \mathbf{B} \times \mathbf{u}$ . Like the electric fields on the accretion disk these fields are not far from cylindrically radial and directed away from the surface of greatest flux,  $P$ , at each height.

We now turn our attention to categorising the different types of solutions. A Helium balloon needs a tether in tension if it is not to rise further. A water tank needs a support in compression if it is not to fall. If we cut a magnetic tower by a horizontal plane there is net tension across that plane due to the magnetic stresses if  $\int (B_z^2 - B_R^2 - B_\phi^2) dA / (8\pi) > 0$  and net compression if that quantity is negative. We call these floaters or pushers respectively if they satisfy those criteria low down the tower. Floaters are held down by magnetic tension; pushers are supported from the bottom by a net magnetic pressure. In the tall tower approximation the above criterion simplifies to  $(\langle B_z^2 \rangle - \langle B_\phi^2 \rangle) > 0$  for a floater. Comparing this criterion with equations (10) and (42) we see floaters have  $s > 1, \nu > 1, \alpha > 1$  and cavities whose radii increase at greater heights while pushers have  $0 < s \leq 1, 0.5 < \nu \leq 1$  and  $0 < \alpha \leq 1$ . Their cavities' radii decrease with height. In a constant pressure medium all the solutions are pushers. If the pressure in a long narrow column supporting a weight is greater than the ambient pressure in the medium surrounding the column then any lateral bend bowing the column will be exaggerated as in the Euler strut problem. All our magnetic towers are stable against that bowing as their net support is atmospheric or less  $(\langle B_R^2 \rangle + \langle B_\phi^2 \rangle - \langle B_z^2 \rangle) / (8\pi) - p = A^{-1} \int A(dp/dz) dz \leq 0$ . This criterion corresponds to  $\alpha \geq 0, s \geq 0$ . Thus squirmers do not occur in the magnetostatics of our systems which have pressure that decreases with height.

## 6 EXACT SOLUTIONS, BACKWARDS METHOD

Here we postulate the forms of  $\beta(P)$  and of the bounding surface  $S$  for which we can solve the differential equation (3). After we have solved it we discover what problem we have solved by finding  $p(z)$  on the bounding surface and the twist angles  $\Phi(P)$  and the boundary flux  $P(R, 0)$ . The differential operator on the left of equation (3) separates in oblate or prolate spheroidal and rotational parabolic coordinates as well as in cylindrical and spherical polars. It is therefore important to take



the surface  $S$  to be one of those coordinate surfaces. Even after choosing one of those the problem is still non-linear; but there are interesting exceptions. We have already seen that the case  $\beta'\beta = \text{const.}$  corresponds to a constant external pressure and it gives a linear but inhomogeneous equation. A second simple case is  $\beta(P) \propto P \propto \beta'\beta$ . This linear case is well known and much explored but is somewhat less interesting than the  $\beta \propto P^{1/2}$  case. The combination  $\beta'\beta \propto P + P_0$  though soluble has the idiosyncrasies of both the former cases without obvious advantages. A different approach with more interesting solutions is to accept the non-linear behaviour of equation (3) and look for self-similar solutions. Most of the above methods can be generalised using perturbation theory. For example if the bounding surface is a ‘cylinder’ of slowly varying radius  $R_m(z)$  one can solve the problem in terms of the scaled radius  $R/R_m$  as in section 4.

### 6.1 SELF-SIMILAR SOLUTIONS

Writing equation (3) in spherical polar coordinates  $(r, \theta, \phi)$  and setting  $\mu = \cos \theta$  we find

$$r^2 \partial^2 P / \partial r^2 + (1 - \mu^2) \partial^2 P / \partial \mu^2 = -r^2 \beta' \beta(P). \quad (63)$$

Self-similar solutions only occur when  $P \propto r^{-l}$ ,  $\beta(P) = C_1 P^\nu$ .

If we now set  $P = r^{-l} M(\mu)$  then the left hand side is  $r^{-l}$  times a function of  $\mu$  so  $\beta'\beta$  which is a function of such a product, must equal such a product. Hence  $\beta'\beta = (1 + 1/l) C_1^2 P^{1+2/l}$ . Thus with  $\nu = 1 + 1/l$  the  $r^{-l}$  cancels out and writing  $f = M/M_1$ , where  $M_1$  is the maximum value of  $M$

$$l(l+1)f + (1 - \mu^2) d^2 f / d\mu^2 = -(1 + 1/l) C_3^2 f^{1+2/l}. \quad (64)$$

This is a version of the equation of Lynden-Bell and Boily (paper 1) for whom the case with  $l$  small was of especial interest.

To make contact with the work of section 4 we remark that for narrow jets it is only necessary to consider  $\mu$  close to one. Supposing the walls at  $\mu = \mu_m$ , we write  $\lambda = (1 - \mu)/(1 - \mu_m)$ , where both  $(1 - \mu_m)$  and  $(1 - \mu)$  are small, the equation takes the form

$$\lambda d^2 f / d\lambda^2 + l(l+1)(1 - \mu_m) f / 2 = -C^2 (1 + 1/l) f^{1+2/l}. \quad (65)$$

We have approximated  $1 - \mu^2$  as  $2(1 - \mu)$ , which is good to 1 per cent or better for opening angles of less than 23 degrees. When the  $(1 - \mu_m)l(l+1)f/2$  is neglected this equation will be recognised as equation (38) of section 3. The particular solutions of equation (64) to which we now turn are so simple that we obtain them without making this narrow cone approximation.

### 6.2 THE DUNCE’S CAP MODEL

Unexpectedly we shall use spherical polar coordinates centred at the top of the tower-like magnetic cavity at  $(0, 0, Z)$ . This use of  $Z$  is similar to the very crude description as a cylindrical tower in the introduction but now the tower will be conical pointing down at the accretion disk. This  $Z$  corresponds to  $Z_h$  in sections 3 and 4. We measure  $\theta$  from the downward axis pointing toward the centre of the accretion disk (see Figure 6). We solve the force free equations within the downward opening cone  $\cos \theta \geq \mu_m$  which forms a dunce’s cap configuration over the accretion disk. We take  $l = -2$  which corresponds to our  $\beta \propto P^{1/2}$  behaviour appropriate for a constant pressure. Equation (64) becomes  $2f + (1 - \mu^2) d^2 f / d\mu^2 = -C_4$ . Writing  $f = (1 - \mu^2)m$  our equation becomes

$d/d\mu[(1 - \mu^2)^2 dm/d\mu] = -C_4$ , so, using the boundary condition that  $(1 - \mu^2)m'$  is non-singular at  $\mu = 1$ , we find,  $m = C_4 \int (1 + \mu)^{-2} (1 - \mu)^{-1} d\mu$ . On integration by parts we get

$$P = r^2 (1 - \mu^2) m = C_4 r^2 (1 - \mu^2) \left[ \frac{1}{2} (1 + \mu_m) - \frac{1}{2} (1 + \mu) + \frac{1}{4} \ln \left( \frac{1 + \mu}{1 + \mu_m} \cdot \frac{1 - \mu_m}{1 - \mu} \right) \right]. \quad (66)$$

Evidently  $P = 0$  on  $\mu = \mu_m$  and on the axis. For tall narrow cones  $\theta$  is small,  $\mu, \mu_m$  are near one and the flux function becomes  $P = \frac{1}{4} C_4 r^2 \theta^2 [\ln(\theta_m^2/\theta^2)]$ . At  $r = Z$  the maximum value of  $P$  is  $F$  so  $C_4 = 4eF/R_d^2$  where  $R_d = \theta_m Z$ . Also  $\beta(P) = \sqrt{2|C_4|} P^{1/2} = C_4 r \theta [\ln(\theta_m/\theta)]^{1/2}$ . Also, see Figure 7,

$$2\pi B_r = (r^2 \theta)^{-1} \partial P / \partial \theta = C_4 [\ln(\theta_m/\theta) - 1]; \quad 2\pi B_\theta = C_4 \theta \ln(\theta_m/\theta); \quad 2\pi B_\phi = C_4 [\ln(\theta_m/\theta)]^{1/2} \quad (67)$$

The constant  $C_4$  is determined by the external pressure  $C_4 = 8\pi[\pi p]^{1/2}$ . Near the axis these fields have precisely the same behaviour as those we found in equations (49) and (50). However the fields are in one sense even more interesting; they are all independent of  $r$ , the distance from the origin. By construction  $B_\theta, B_\phi$  vanish at the edge of the cone but  $B_r$  is constant along its generators all the way up to the origin. The origin itself is then a point at which the infinite field coming up the axis turns back and splays out down these generators at constant field strength. This is the way the constant external pressure is opposed. With the origin such a remarkable point, some may suspect that the forces do not balance there, that the whole configuration might be held up by some sky-hook pulling at the apex. However  $P$  varies as  $r^2$  and the Maxwell

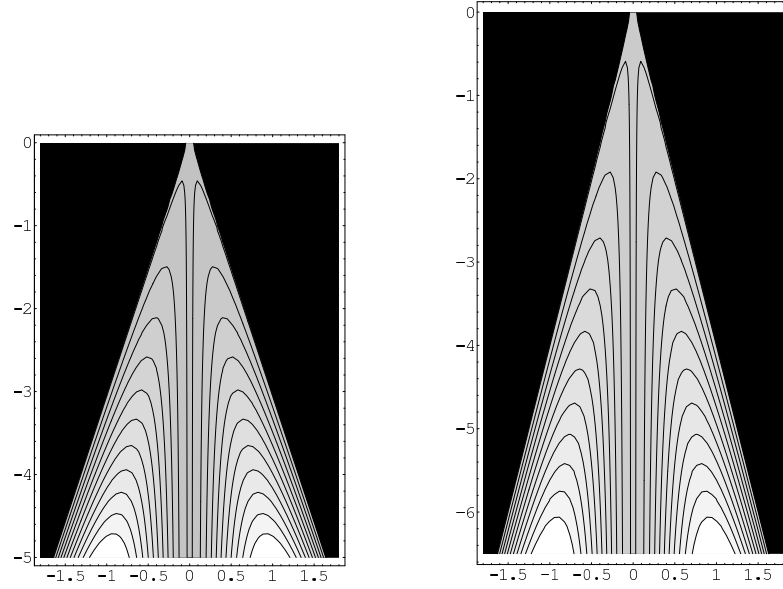


**Figure 6.** The poloidal lines of force in the Duncce's cap model at two different times. The top advances at constant speed while the bottom only revolves in differential rotation

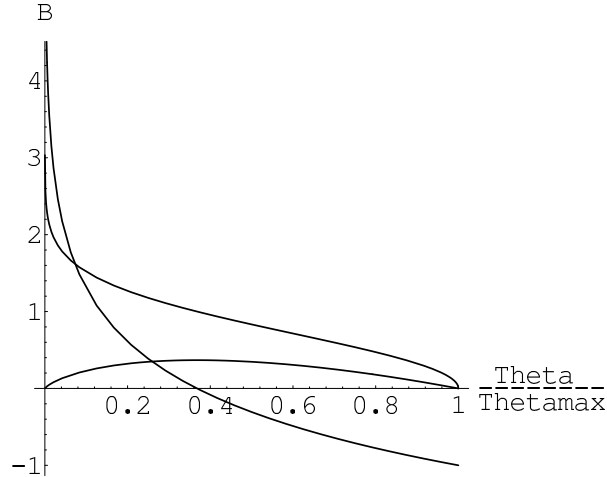


**Figure 7.**  $B_r$ ,  $B_\theta$  and  $B_\phi$  are all independent of  $r$  inside the Duncce's Cap so we plot them as functions of  $\theta/\theta_{max}$ . While  $B_\theta$  is zero at both boundaries  $B_\phi$  is zero only at the outer one.  $B_r$  passes through zero at an internal point. See text for the surprising behaviour near  $\theta = 0$

stresses integrated over horizontal cuts through the cone give a net force that vanishes like  $r^2$  as the origin is approached. Thus no sky hook is necessary to balance forces at the origin. The radial fields reverse at an intermediate value  $\theta_1 = \theta_m/\sqrt{e}$  (for narrow cones) and some may suspect reconnection there but the  $B_\phi$  field component maximises at that value of theta so there is plenty of magnetic pressure to prevent reconnection. With  $\mu_m$  close to one the radii on the accretion disk are  $R = \theta Z$  so the flux coming up within a circle of radius  $R$  is  $P(R, 0) = Fe(R^2/R_d^2)[\ln(R_d^2/R^2)]$ . The twist function  $\Phi(P)$  is given by integration along field lines which is simple for this self-similar field.  $rd\theta/B_\theta = r \sin \theta d\phi/B_\phi$  yields on writing  $\eta = \theta_m/\theta$

$$\Phi(P) = \Omega(P)t = (Z/R_d) \int_{\eta_i}^{\eta_o} (\ln \eta)^{-1/2} d\eta \simeq (Z/R_d) [(\eta_i - \eta_o)(\ln \eta_i)^{-1/2}], \quad (68)$$

where the integral is evaluated between foot points at  $R_{i,o}(P)$  of the field line and  $\eta_{o,i}(P) = R_d/R_{o,i}(P)$ . Therefore  $\eta_{o,i}$  are the roots for  $\eta$  of

$$P/F = 2e\eta^{-2} \ln \eta \quad (69)$$

When the inner foot is much further in than the outer foot then  $\Omega_i \gg \Omega_o$  so then  $\Omega(P)$  is close to  $\Omega_i(P)$ . This allows us to estimate the angular velocity of the accretion disk required. In the central parts it behaves as  $R^{-1}[\ln(R_d/R)]^{-1/2}$ , so the circular velocity of the disk is almost constant but drops to zero at the very centre like  $[\ln(R_d/R)]^{-1/2}$ . From Equation (69) both roots  $\eta_{o,i}$  are independent of time. Hence from equation (68)  $Z \propto t$  as expected from section 4 so we may write  $Z = Vt$ . Writing our solution for  $P$  in terms of cylindrical polar coordinates now centred on the centre of the disk,  $P = eF(R^2/R_d^2) \ln(R_m^2/R^2)$ , where  $R_m(z) = R_d(1 - z/Z)$  for  $z < Z$  and it is just the dependence of  $Z$  on time that generates the evolution of the system.  $\beta(P) = \sqrt{8eFP^{1/2}}/R_d$  with  $\Phi(P)$  given by equation (69). The magnetic fields are given by equation (67) so we now calculate the electric fields following the method of section 5. The simplicity of the expression for  $P$  means that  $q$  is simpler and in place of equation (60) we have  $\phi = \psi + \Omega_d(R_o)t + (Vt/R_d) \int_{\eta_o}^{R_m/R} (\ln \eta)^{-1/2} d\eta$ . Now  $R_m = (1 - \frac{z}{Vt})R_d$  so  $\dot{R}_m = zR_d/(Vt^2)4$ . At fixed height a point only remains on the same field line if  $\dot{R} = -\dot{P}/(\partial P/\partial R) = -\dot{P}/(2\pi R B_z)$  Using these and differentiating  $\phi$  at constant  $z$  and  $P$

$$\dot{\phi} = \Omega_d + V R_d^{-1} \int_{\eta_o}^{R_m/R} (\ln \eta)^{-1/2} d\eta + [\ln(R_m/R)]^{-1/2} \left( \frac{z}{Rt} + \frac{\dot{P} V t}{2\pi R_d R^3 B_z} \right). \quad (70)$$

As before Equations (61) and (62) give the velocities of the lines of force as,

$$\begin{aligned} u_\phi &= [(B_R^2 + B_z^2)/B^2] R \dot{\phi} + [B_R B_\phi / (B^2 B_z)] \dot{P} \\ u_R &= [B_z^2 / (B_R B_\phi)] [R \dot{\phi} - u_\phi (1 + B_\phi^2/B_z^2)] \\ u_z &= (B_z/B_R) u_R + \dot{P}/B_R \end{aligned} \quad (71)$$

Also  $cE_\phi = -\dot{P}/(2\pi R)$  while the other components follow from  $c\mathbf{E} = \mathbf{B} \times \mathbf{u}$ . Notice that the meridional field velocity  $\mathbf{u}_M = (u_R, u_z)$  is not perpendicular to the vector meridional component of the magnetic field. It is the full vector velocity that is perpendicular to the complete magnetic field. We have explored the Duncie's Cap model in all this detail both to demonstrate its interesting field structure and to show how we get the fields in an explicit example. Figure 5 gives the poloidal structure of the magnetic fields which wind around these surfaces of constant flux.

## 7 CONCLUSIONS

It is very remarkable that these simple analytic methods allow the solution of these highly non-linear problems with variable domain, not just for a few special cases but for all twist functions  $\Omega$  and all pressure distributions. Furthermore we get time-dependent solutions for all time. The main secret lies in the variational principle coupled with a good form of trial function. Once the time-dependence becomes relativistic we lose this tool so the problems will become harder. However when the relativistic motion is only important for the rotation it is likely that another variational principle may exist. An important problem is to seek it out. In the foregoing we have explored the simplest case in which the magnetic cavity is empty and the Poynting flux carries both the energy and the momentum of the jet. I believe that the results justify the assertion that this simplest case has remarkable similarities to the observed world and this suggests that the extra complication of material winds is not essential to explaining the main phenomena. However especially for Pulsars Relativistic rotation is an essential ingredient of the problem not covered here.

## 8 ACKNOWLEDGMENTS

We are grateful to the Institute of Advanced Study for providing the environment at Princeton where much of this work was done thanks to the support of the Monell Foundation. It was started earlier on a visit to the Carnegie Observatories in Pasadena where most of paper III was completed. Discussions with N.O.Weiss and P.Goldreich proved most helpful; C.Pichon and G.Preston helped with computations and F.J. Dyson was a source of encouragement.

## REFERENCES

Appl, S., Lery, T. & Baty, H., 2000, A&A, 355, 818

- Baade, W., 1956, *ApJ*, 439, L43
- Bardeen, J., 1970, *Nature*, 226, 64
- Begelman, M.C., Blandford, R.D. & Rees, M.J., 1984, *Revs Mod Phys*, 56, 255
- Blandford, R.D. & Payne, D.G., 1982, *MNRAS*, 199, 883
- Bogovalov & Tsinganos, K., 2002, *MNRAS*, 325, 249
- Bogovalov & Tsinganos, K., 2002, *MNRAS*, 337, 553
- Cohen, M., Van Winckel, H., Bond, H.E. & Gull, T.R., 2004, *A.J.*, 127, 2362
- Curtis H.D., 1918, *Pub Lick Observatory*, 13, 31
- Genzel, R., Schödel, R., Olt, T., Eckart, A., Alexander, T., Lacombe, F., Rouan, D. & Aschenback, B., 2003, *Nature*, 425, 934
- Ghez, A.M. et al., 2004, *ApJ*, 601, L159
- Gizani, N.A.B. & Leahy, J.P., 2003, *MNRAS*, 342, 399
- Gull, S.R. & Northover, F.J.E., 1976, *Nature*, 263, 572
- Hazard, C., Mackey, M.B. & Shimmins, T.A.R., 1963, *Nature*, 197, 1037
- Heyvaerts, J. & Norman, C.A., 2003, *ApJ*, 596, 1240, 1256, 1270
- Kormendy, J. & Richstone, D., 1995, *Astron Rev of A & A*, 33, 581
- Kronberg, P.P., Colgate, S.A., Li, H. & Dufton, Q.W., 2004, *ApJ*, 604, L77
- Lebedev, S.V., Ciardi, A., Ampleford, D.J., Bland, S.N., Bott, S.C., Chittenden, J.P., Hall, G.N., Rapley, J., Jennings, C.A., Frank, A., Blackman, E.G. & Lery, T., 2005, *MNRAS*, 361, 97L
- Leblanc, J.M. & Wilson, J.R., 1970, *ApJ*, 161, 541
- Lery, T., Baty, H. & Appl, S., 2000, *A&A*, 355, 1202
- Li, H., Lapenta, G., Finn, J.M., Li, S. & Colgate, S.A., 2006, preprint
- Lovelace, R.V.E., 1976, *Nature*, 262, 649
- Lovelace, R.F.E., Li, H., Koldoba, A.V., Ustyugova, G.V. & Romanova, M.M., 2002, *ApJ*, 572, 445
- Lovelace, R.V.E. & Romanova, M.M., 2003, *ApJ*, 596, L159
- Lynden-Bell, D., 1969, *Nature*, 223, 690
- Lynden-Bell, D. & Boily, C., 1994, *MNRAS*, 267, 146 (Paper I)
- Lynden-Bell, D., 1996, *MNRAS*, 279, 389 (Paper II)
- Lynden-Bell, D. & Rees, M.J., 1971, *MNRAS*, 152, 461
- Lynden-Bell, D., 2001, in Knapen J.H. *et al.* eds. *ASP Conf. Vol. 249*, 212
- Lynden-Bell, D., 2003, *MNRAS*, 341, 1360 (Paper III)
- Mestel, L., 1999, *Cosmical Magnetism*, Oxford
- Michalitsanos, A.G., Oliverson, R.J., Kafatos, M., Gull, H.E. & Miller, R.J., 1988, *A.J.*, 95, 1478
- Mirabel, T.F. & Rodriguez, L.F., 1999, *ARA&A*, 37, 409
- Miyoshi, M., Moran, J., Hernstein, J., Greenhill, L., Nakai, N., Diamond, P. & Inoue, M., 1995, *Nature*, 373, 127
- Ouyed, R., Clarke, D.A. & Pudritz, R.E., 2003, *ApJ*, 582, 292
- Prendergast, K., 2005, *MNRAS*, 359, 725
- Pudritz, R.E., Rogers, C.S. & Ouyed, R., 2006, *MNRAS*, 365, 1131
- Rees, M.J., 1971, *Nature*, 229, 312
- Ryle, M., 1968, *IAU Highlights of Astronomy*, Ed. L.Perek, D.Reidel
- Sakurai, R., 1987, *PASJ*, 39, 821
- Salpeter, E.E., 1964, *ApJ*, 140, 796
- Schott, G.A., 1912, *Electromagnetic Radiation & Reactions arising from it*, Cambridge University Press, Cambridge
- Schmidt, M., 1963, *Nature*, 197, 1040
- Shakura, N.I. & Sunyaev, R.A., 1973, *Astron & Astrophys*, 24, 37
- Shakura, N.I. & Sunyaev, R.A., 1976, *MNRAS*, 173, 613
- Shibata, K. & Uchida, Y., 1985, *Pub Astron Soc Japan*, 37, 31
- Shibata, K. & Uchida, Y., 1986, *Pub Astron Soc Japan*, 38, 637
- Stalin, C.S., Gupta, A.C., Gopal Krishna, Gopal Krishna, Wiita, P.J. & Sagar, R., 2005, *MNRAS*, 356, 2004
- Thompson, C., Lyutikov, M. & Kulkarni, S.R., 2002, *ApJ*, 574, 332
- Uzdensky, D.A. & MacFadyen, A.I., 2006, preprint
- Vinković, D., Blöcker, T., Hofmann, K.H., Elitzur, M. & Weigelt, G., 2004, *MNRAS*, 352, 852
- Vlemmings, W.H.T., Diamond, P.J. & Imai, H., 2006
- Wheeler, J.A., 1971, in *Nuclei of Galaxies*, Ed. D.J.K. O'Connell, Pontifical Acad Sci

## APPENDIX A: A USEFUL MATHEMATICAL TECHNIQUE

We wish to solve a highly non-linear differential equation such as

$$(1 - \mu^2) \frac{d^2 f}{d\mu^2} = -l(l+1)f - C^2 \nu f^{2\nu-1} ; \quad \nu = 1 + \frac{1}{l} \quad (\text{A1})$$

under the boundary conditions that  $f$  is zero at given end points and that  $C$  is so chosen that the maximum of  $f$  is one. There should be only one maximum of  $f$  between the end points. We rewrite the equation in the form

$$(1 - \mu^2) \frac{d}{d\mu} \left( \frac{df}{d\mu} \right)^2 = \frac{d}{d\mu} S^2 \quad (\text{A2})$$

where

$$S^2 = l(l+1)(1 - f^2) + C^2(1 - f^{2\nu}) . \quad (\text{A3})$$

We shall be particularly interested in the strongly non-linear case with  $\nu$  large ( $l$  small) so we start with  $\nu$  large but later extend the technique down to  $\nu \approx 1$ . As we shall come across several variants of essentially the same problem we describe the technique in terms of the more general problem in which A2 is replaced by

$$G(\mu) \frac{d}{d\mu} \left( \frac{df}{d\mu} \right)^2 = \frac{d}{d\mu} [S(f)]^2 \quad (\text{A4})$$

with  $S^2(f)$  zero when  $f$  reaches its maximum of 1. We shall assume that  $S(f)$  depends on parameters such as  $\nu$  or  $C$  in (A1) and that we are primarily interested in the solution when  $\nu$  is large in which case  $dS^2/df$  is strongly peaked close to  $f = 1$  and away from there it is small. Under these conditions (which hold for (A1)) most of the deceleration  $-d^2 f/d\mu^2$  of  $f$  occurs in the region in which  $f$  is close to one. Let that maximum be at  $\mu = \mu_1$ . Then at  $\mu_1$

$$(d^2 f/d\mu^2)_1 = \frac{1}{2G_1} \left[ \frac{dS^2}{df} \right]_1 = -g \text{ say} \quad (\text{A5})$$

where  $G_1 = G(\mu_1)$ . Near  $\mu = \mu_1$

$$f = 1 - \frac{1}{2}g(\mu - \mu_1)^2 \quad (\text{A6})$$

and  $S^2 = (dS^2/df)_1(f - 1)$  so

$$\mu - \mu_1 = G_1^{-1/2} g^{-1} S \quad (\text{A7})$$

$$G(\mu) \simeq G_1 + G'_1(\mu - \mu_1) \simeq G_1(1 + a_1 S)^3 \quad (\text{A8})$$

where

$$a_1 = \frac{1}{3} G'_1 G_1^{-3/2} g^{-1} \quad (\text{A9})$$

and  $G'_1 = (dG/d\mu)$  at  $\mu_1$ .

Writing (A8) as a cubic leads to simpler mathematics later. Near  $\mu = \mu_1$  where most of the ‘deceleration’ of  $f$  takes place we see from (A4) that

$$\frac{d}{d\mu} \left( \frac{df}{d\mu} \right)^2 = \frac{2S dS/d\mu}{G_1(1 + a_1 S)^3} \quad (\text{A10})$$

We have derived this equation near  $\mu = \mu_1$  but away from there  $f^{2\nu}$  is small and as  $dS^2/d\mu$  is small and  $1 + a_1 S$  is not near zero, the equation can be taken to hold everywhere. We now integrate (A10) and remembering that  $df/d\mu$  is zero at  $\mu_1$  we find

$$(df/d\mu)^2 = \frac{S^2}{G_1(1 + a_1 S)^2} \quad (\text{A11})$$

It was to get this simple result that we chose the cubic form in (A8). Taking the square root and multiplying up by  $1/S + a_1$  we find

$$\int_{\mu}^{\mu_1} \frac{df}{S} + a_1(1 - f) = G_1^{-1/2}(\mu - \mu_1) \quad (\text{A12})$$

To proceed further we must integrate  $df/S(f)$ . As the major item in (A1) is  $f^{2\nu-1}$  we shall assume that near the maximum of  $f$ ,  $S^2$  can be approximated as  $C_1^2(1 - f^{2\nu})$ . We do this by taking

$$\bar{\nu} = \frac{1}{2} [d \ln[S^2(0) - S^2]/d \ln f]_{f=1} \quad (\text{A13})$$

and

$$C_1^2 = gG_1/\bar{\nu} \quad (\text{A14})$$

We now use the method of paper I to give us  $\int (1 - f^{2\bar{\nu}})^{-1/2} df$  for large  $\bar{\nu}$ .

Set  $f = 1 - \frac{1}{\bar{\nu}} \ln q$ ;  $df = -\frac{1}{\bar{\nu}} \frac{dq}{q}$ . Then  $f^{2\bar{\nu}} = (1 - \frac{1}{2\bar{\nu}} \ln q^2)^{2\bar{\nu}} \rightarrow \exp -(\ln q^2) = 1/q^2$  so  $\int (1 - f^{2\bar{\nu}})^{-1/2} df = \frac{1}{\bar{\nu}} \int (q^2 - 1)^{-1/2} dq = \frac{1}{\bar{\nu}} ch^{-1} q$  so setting  $q = ch\Lambda$  we find

$$f = 1 - \frac{1}{\bar{\nu}} \ln(ch\Lambda) \quad (\text{A15})$$

and from (A12)  $\Lambda$  is given by

$$\Lambda + a_1 C_1 \ln(ch\Lambda) = \bar{\nu} C_1 G_1^{-1/2} (\mu - \mu_1) \quad (\text{A16})$$

and we remember that  $a_1 = \frac{1}{3} G_1' G_1^{-3/2} g^{-1} = \frac{1}{3} \frac{G_1'}{G_1^{1/2} \bar{\nu} C_1^2}$ . To complete the solution we must impose the boundary conditions and so find the value of  $C$  needed to make  $f$  one at its maximum. However the boundaries vary from one application to another so it is time to consider the differential equations and their ranges one by one.

The application in this paper is to the solution of equation (38)  $\lambda d^2 f / d\lambda^2 = -C^2 \nu f^{2\nu-1}$ .

To use the general theory above for this equation we write  $\lambda$  for  $\mu$  and  $G(\lambda) = \lambda$ ,  $G_1 = \lambda_1$  and  $S^2 = C^2(1 - f^{2\nu})$  the boundaries are at  $\lambda = 0$  and  $\lambda = 1$  and  $\bar{\nu} = \nu$ ,  $C = C_1$ . At those boundaries we need  $ch\Lambda = e^\nu$  so that  $f = 0$ . If  $\Lambda_1$  is the positive value of  $\Lambda$  satisfying this then the negative solution is  $-\Lambda_1$  so at  $\lambda = 1$  and  $\lambda = 0$  respectively  $\Lambda_1 + a_1 C \nu = \nu C \lambda_1^{-1/2} (1 - \lambda_1) - \Lambda_1 + a_1 C \nu = -\nu C \lambda_1^{1/2}$  where  $a_1 = \frac{1}{3\lambda_1^{1/2} \nu C^2}$ .

Subtracting  $2\Lambda_1 = \nu C \lambda_1^{-1/2}$

adding  $a_1 C \nu = \nu C \lambda_1^{-1/2} (\frac{1}{2} - \lambda_1) = 2\Lambda_1 (\frac{1}{2} - \lambda_1)$  so using the value of  $a_1$  above and eliminating  $C$

$$\lambda_1 \left( \frac{1}{2} - \lambda_1 \right) = \nu / (12\Lambda_1^2)$$

Now  $\Lambda_1 \simeq \nu$  or more accurately  $\nu \left( 1 + \frac{\ln 2 - \frac{1}{2} e^{-2\nu}}{\nu} \right)$  so the quantity on the right is  $0 \left( \frac{1}{12\nu} \right)$  which is small so  $\lambda_1$  is nearly a half. Accurately

$$\lambda_1 = \frac{1}{2} \left[ \frac{1 + \sqrt{1 - \frac{4\nu}{3\Lambda_1^2}}}{2} \right] \quad (\text{A17})$$

with  $\lambda_1$  known

$$C = 2\lambda_1^{1/2} \Lambda_1 / \nu \quad (\text{A18})$$

This completes the solution when  $\nu$  is large

$$f \simeq 1 - \frac{1}{\nu} \ln \left\{ ch \left\{ 2\Lambda_1 (\lambda - \lambda_1) - \frac{1}{6\Lambda_1} \{ \ln ch [2\Lambda_1 (\lambda - \lambda_1)] \} \right\} \right\} \quad (\text{A19})$$

## A1 Solutions when $\nu$ is no longer large

When  $\nu$  is lowered the solution will still have a single hump and will still fall to zero at the end points but it will no longer have precisely the form given in (A15), (A16) because there will be more deceleration of  $f$  away from  $\mu = \mu_1$  where our approximations for  $G(\mu)$  and  $S(f)$  are no longer valid. To allow for this we generalise the form of (A16) and (A17) to

$$f = 1 - \frac{1}{H} \ln ch\Lambda \quad (\text{A20})$$

$$\Lambda + \Delta \ln ch\Lambda = hCG_1^{-1/2} (\mu - \mu_1) \quad (\text{A21})$$

where  $H$  and  $h$  can now be different and only for  $\nu$  large will they become equal to  $\nu$ . Furthermore  $\Delta$  is no longer restricted to the form it took previously in terms of  $a_1$ ,  $\nu$  and  $C$ . We show in this section that with the four parameters  $H$ ,  $\Delta$ ,  $h$   $C$  and  $\mu_1$  we can ensure that the solution has the right position of the maximum, the right deceleration there and that the gradients of the solution at the end points are appropriate for the differential equation. Since the desired solution has just one hump and is zero at the end points it is no surprise that we can fit it well not only for  $\nu$  large but for  $\nu > 1$ . In practice we find errors from computed solutions are less than 1% rising above 2% for  $\nu = 1$ . Since  $C$  is itself to be determined from the fitting of boundary conditions in the original equation we have actually five constants  $H$ ,  $\Delta$ ,  $h$ ,  $C$  and  $\mu_1$  to be determined so we impose the following five conditions on our proposed form of solution A

$$1/ \& 2/ f = 0 \text{ at the end points so there } ch\Lambda_1 = e^H \quad (\text{A22})$$

$$3/ - \frac{d^2 f}{d\mu^2} = -\frac{1}{2G_1} \left( \frac{dS^2}{df} \right)_{f=1} \quad \text{this gives } \frac{h^2 C^2}{H} = \frac{1}{2} \left. \frac{dS^2}{df} \right|_1 \quad (\text{A23})$$

As we wish our proposed solution to solve (A4) as nearly as possible we now integrate (A4) by parts first from  $\mu_1$  to 1 and then from the lower boundary  $\mu_m$  to  $\mu_1$ . These give us

$$G(1) \left( \frac{df}{d\mu} \right)_{\mu=1}^2 - \int_{\mu_1}^1 \left( \frac{df}{d\mu} \right)^2 G'(\mu) d\mu = [S(0)]^2 \quad (\text{A24})$$

and

$$-G(\mu_m) \left( \frac{df}{d\mu} \right)_{\mu_m}^2 + \int_{\mu_m}^{\mu_1} \left( \frac{df}{d\mu} \right)^2 G'(\mu) d\mu = [S(0)]^2 \quad (\text{A25})$$

We now use the forms (A20) and (A21) and substitute

$$\left( \frac{df}{d\mu} \right)^2 = \frac{1}{H} t h^2 \Lambda \frac{d\Lambda}{d\mu} \frac{hC}{G_1^{1/2} [1 + \Delta t h \Lambda]} \quad (\text{A26})$$

into the integrals in (A24), (A25) but use for the end value in (A25)

$$\left( \frac{df}{d\mu} \right)_{\mu_m}^2 = \frac{1}{H^2} (1 - e^{-2H}) \frac{h^2 C^2}{G_1 [1 - \Delta \sqrt{1 - e^{-2H}}]} \quad (\text{A27})$$

For  $(f')_{\mu=1}^2$  we merely reverse the sign of  $\Delta$  in (A27). We then perform the integrals, so (A22)–(A25) provide us with the five equations to determine our five parameters.

We wrote (A26) in that form because in the application to narrow jets  $G$  is linear so that the integrals are readily performed using  $\Lambda$  as the variable of integration. For that case the integral involved is

$$\begin{aligned} \int \frac{t h^2 \Lambda}{1 + \Delta t h \Lambda} d\Lambda &= \int \frac{1 - \text{sech}^2 \Lambda}{1 + \Delta t h \Lambda} d\Lambda = -\frac{1}{\Delta} (1 + \Delta t h \Lambda) + \int \frac{(e^{2\Lambda} + 1) d\Lambda}{(1 + \Delta) e^{2\Lambda} + 1 - \Delta} \\ &= \frac{-1}{\Delta} \ln(1 + \Delta t h \Lambda) + \frac{\Lambda}{1 - \Delta^2} - \frac{\Delta}{1 - \Delta^2} \ln \left( \frac{1 + \Delta}{1 - \Delta} + e^{-2\Lambda} \right) \end{aligned}$$

Applying these methods to the solution of equation (38), with  $\lambda$  written for  $\mu$  and  $G(\lambda) = \lambda$ ,  $S^2 = C^2(1 - f^{2\nu})$  and boundaries at  $\lambda = 0$  and  $\lambda = 1$  the five equations are with  $\Lambda_1 = ch^{-1}e^H$

$$\Lambda_1 + \Delta \ln ch \Lambda_1 = hC \lambda_1^{-1/2} (1 - \lambda_1) \quad (\text{A28})$$

$$-\Lambda_1 + \Delta \ln ch \Lambda_1 = -hC \lambda_1^{+1/2} \quad (\text{A29})$$

$$h^2/H = \nu \quad (\text{A30})$$

and from (A24) and (A25)

$$C^2 = \frac{1}{H^2} (1 - e^{-2H}) \frac{h^2 C^2}{\Lambda_1 (1 + \Delta \sqrt{1 - e^{-2H}})} - \frac{hC \lambda_1^{-1/2}}{H^2} \left\{ -\frac{1}{\Delta} \ln [1 + \Delta \sqrt{1 - e^{-2H}}] + \frac{\Lambda_1}{1 + \Delta} - \frac{\Delta}{1 - \Delta^2} \ln \left( \frac{1 + \sqrt{1 - e^{-2H}}}{1 + \Delta \sqrt{1 - e^{-2H}}} \right) \right\} \quad (\text{A31})$$

$$C^2 = \frac{hC \lambda_1^{-1/2}}{H^2} \left\{ +\frac{1}{\Delta} \ln(1 - \Delta \sqrt{1 - e^{-2H}}) + \frac{\Lambda_1}{1\Delta} - \frac{\Delta}{1 - \Delta^2} \ln \left( \frac{1 - \sqrt{1 - e^{-2H}}}{1 - \Delta \sqrt{1 - e^{-2H}}} \right) \right\} \quad (\text{A32})$$

In solving these one uses the sum and differences of (29) and (30) and thinks of  $H$  rather than  $\nu$  as the independent variable. Figure 5 demonstrates the accuracy of the results compared with computed solutions.

Finally we rewrite the approximate results as power series in  $\nu^{-1}$

$$H = \nu - 1/42 - 5/26 \cdot \nu^{-1}$$

$$h = \sqrt{H\nu}$$

$$\Delta = 1/2 \cdot \nu^{-1} - 1/9 \cdot \nu^{-2} + 1/12 \cdot \nu^{-3}$$

$$\lambda_1 = 1/2 - 7/31 \cdot \nu^{-1} + 4/41 \cdot \nu^{-2}$$

$$C_* = hC \lambda_1^{-1/2} = 2\nu + \ln 4 - 4/15 \cdot \nu^{-1}$$